Chem Soc Rev

This article was published as part of the

Hybrid materials themed issue

Guest editors Clément Sanchez, Kenneth J. Shea and Susumu Kitagawa

Please take a look at the issue 2 2011 table of contents to access other reviews in this themed issue

Chem Soc Rev

Chemical Society Reviews

www.rsc.org/chemsocrev

Volume 40 | Number 2 | February 2011 | Pages 453–1152

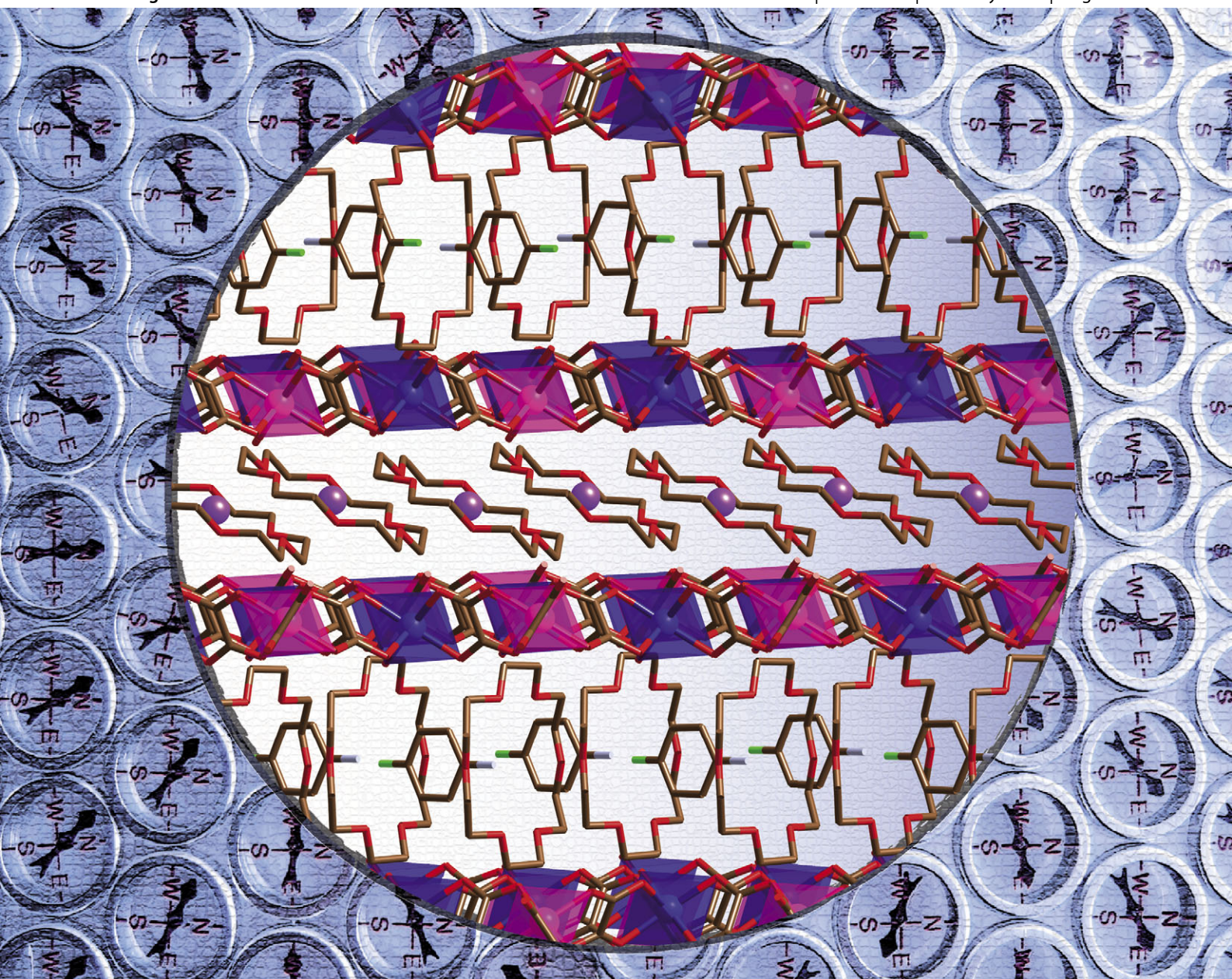

Themed issue: Hybrid materials

ISSN 0306-0012

RSC Publishing

TUTORIAL REVIEW

Miguel Clemente-León, Eugenio Coronado, Carlos Martí-Gastaldo and Francisco M. Romero

Multifunctionality in hybrid magnetic materials based on bimetallic oxalate complexes

Chem Soc Rev

Dynamic Article Links

Cite this: *Chem. Soc. Rev.*, 2011, **40**, 473–497

www.rsc.org/csr

TUTORIAL REVIEW

Multifunctionality in hybrid magnetic materials based on bimetallic oxalate complexes†

Miguel Clemente-León,[ab] Eugenio Coronado,*[a] Carlos Martí-Gastaldo‡[a] and Francisco M. Romero[ab]

Received 15th September 2010
DOI: 10.1039/c0cs00111b

This *tutorial review* illustrates the design of multifunctional oxalate-based magnetic materials through the combination of the intrinsic magnetism of the metal–organic framework and the additional properties introduced by several organic/inorganic functional cations.

Introduction

Over the last three decades, coordination chemists have acquired high control and expertise in the design of supramolecular architectures, whose physical properties and dimensionality are strongly dependent on the nature of their constituent metal complexes and the molecular bridging ligands used to interconnect them in the solid-state. Magnetic molecular materials exemplify this assessment.[1] In the design of these systems the linker plays a key role, as it must provide an effective pathway for the super-exchange interactions. In fact, the majority of molecule-based magnets reported so far are exclusively based on linkers with a small size (constituted by a low number of atoms) while simultaneously offering π and σ electronic pathways for the magnetic super-exchange, such as oxalate ($C_2O_4^{2-}$),[2] oxamate (pbaOH),[3] cyanide (CN^-)[4] or dicyanamide ($[N(CN)_2]^-$).[5] Their synthetic versatility has enabled the design of a myriad of coordination polymers (CPs) that, apart from exhibiting interesting magnetic properties, have demonstrated their ability to incorporate more sophisticated functionalities, thus permitting the design of advanced multifunctional materials such as ferromagnetic conductors,[6] photo and piezo switching magnets,[7–10] chiral magnets,[11–18] or multiferroics,[19–21] amongst others.

Though several reviews dealing with the problem of multifunctionality in magnetic coordination materials have already been published, they have mainly focused on the multifunctional properties of these materials.[22–27] In this review we will follow a different approach as we will exclusively focus on the oxalate ligand to illustrate the potential of the chemical approach to the development of this class of material. In fact, the oxalate dianion has been demonstrated to be one of the most versatile ligands used in the search for molecule-based

[a] *Universidad de Valencia (ICMol), Catedrático José Beltrán 2, 46980 Paterna, Spain. E-mail: eugenio.coronado@uv.es; Fax: +34 96.354.32.73; Tel: +34 96.354.44.15*
[b] *Fundación General de la Universidad de Valencia (FGUV), Amadeu de Saboia 4, 46010 Valencia, Spain*
† Part of the themed issue on hybrid materials.
‡ Present address: Department of Chemistry, University of Liverpool, Crown Street, Liverpool, L69 7ZD, UK.

Miguel Clemente-León

Miguel Clemente-León obtained a PhD in Chemistry at the University of Valencia in 1999 under the supervision of Prof. E. Coronado. From 2000 to 2002 he was a postdoctoral researcher in the group of Prof. V. Balzani at the University of Bologna. Since 2002 he has been a researcher at ICMol (University of Valencia). He is currently working on the design of multifunctional magnetic materials incorporating spin-crossover complexes and in the fabrication of LB films based on functional molecules.

Eugenio Coronado

Eugenio Coronado has been Professor of Inorganic Chemistry at the University of Valencia since 1993 and Director of the University's Institute of Molecular Science (ICMol) since its foundation in 2000. He is the author of numerous contributions in molecular magnetism, with particular emphasis on the chemistry and physics of multifunctional molecular materials and nanomagnets. Currently, his research is focused on the use of these magnetic materials in molecular spintronics.

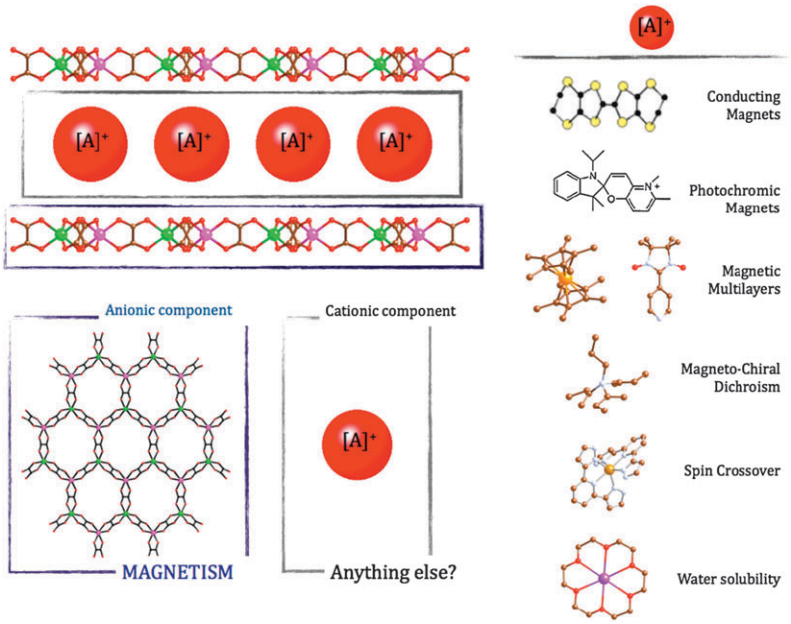

Fig. 1 Scheme illustrating the chemical approach towards the development of layered 'dual-function' oxalate-based materials.

magnets. In its bis-bidentate chelate form, the topology and dimensionality of the coordination lattice, as well as the sign and anisotropy of the magnetic exchange can be controlled at will, allowing for the preparation of a large variety of tunable magnetic frameworks. Furthermore, these frameworks are negatively charged and therefore can be combined with functional molecular cations in order to afford hybrid salts combining cooperative magnetism with a second property of interest. A remarkable example of chemically-designed multifunctionality is provided by the preparation of hybrid materials combining ferromagnetism with metal-like conductivity.[6,23,28,29] This review aims to illustrate the versatility of this hybrid approach towards the development of novel multifunctional materials by focusing on more recent examples, which rely on the combination of these negatively charged oxalate-based bimetallic magnetic lattices with (a) cationic radicals to produce hybrid organic/inorganic magnetic heterospin networks; (b) spin-crossover complexes, which enable the design of switching magnets; and (c) crown ether complexes, which introduce water-solubility to these magnetic CPs (Fig. 1).

Chemical and structural aspects for the design of bimetallic oxalate-based magnetic architectures

Most of the oxalate-based molecular magnets described so far have been obtained by following the so-called '*complex-as-ligand approach*'. In this synthetic strategy a molecular building block, the homoleptic $[M^{III}(ox)_3]^{3-}$ (M^{III} = Cr, Fe, Ru, Rh, Mn or V) tris-oxalate metalate octahedral complex, is used as a ligand towards divalent metal cations. Their combination results in the formation of low-dimensional anionic complexes, which remain in solution due to their charged nature. Next, the addition of a bulky organic cation, *i.e.* $[XR_4]^+$, pushes these anionic moieties to

Carlos Martí-Gastaldo

Carlos Martí-Gastaldo earned his PhD in Chemistry in 2009 at the Universidad de Valencia (ICMol) under the supervision of Prof. E. Coronado and Dr J. R. Galán-Mascarós in the field of molecular and solid-state multifunctional magnetic materials. After receiving a Marie Curie Fellowship, he has recently joined the group led by Prof. M. J. Rosseinsky at the University of Liverpool to explore the design of advanced multifunctional metal–organic frameworks.

Francisco M. Romero

Francisco M. Romero received his PhD in 1997 from the Université Louis Pasteur (ULP) de Strasbourg under the supervision of Drs Marc Drillon and Raymond Ziessel. Then he joined the group of Prof. Decurtins (Department für Chemie und Biochemie, University of Berne) as a post-doctoral researcher. Since 1999 he has been working as a researcher at ICMol (University of Valencia). His research interests cover different aspects of molecular magnetism, ranging from single-molecule magnets and nanomagnetism to switchable magnetic materials.

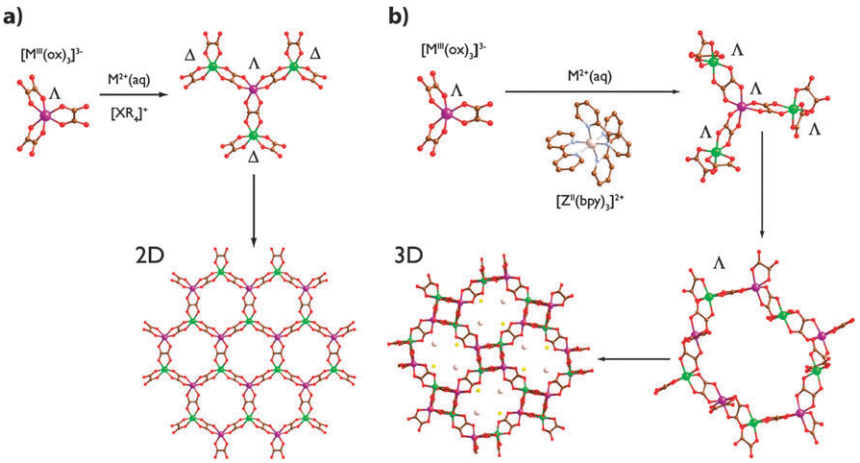

Fig. 2 Diagram illustrating the formation of 2D heterochiral (a) and 3D homochiral (b) oxalate-based architectures depending on the nature of the cation used to template their assembly.

self-assemble resulting in the precipitation of non-soluble CPs (Fig. 2a). The first example in this direction was reported by Okawa in the beginning of the 90s, with the synthesis of a family of 2D layered honeycomb-like magnets with general formula: $[XR_4][M^{II}Cr(ox)_3]$ ($XR_4^+ = NBu_4^+$; M^{II} = Mn, Fe, Co, Ni, Cu, Zn), which presented ferromagnetic ordering from 6 to 12 K.[30] Soon after this discovery, the use of other trivalent metals yielded analogous layered molecular magnets showing ferro-, ferri- and weak ferromagnetic ordering with critical temperatures up to 45 K.[31–37]

In these compounds monovalent cations not only act as charge-compensating counterions, they also act as templating agents that control the dimensionality of the final system. This point is exemplified by the substitution of the monocations of the type $[XR_4]^+$ with tris,bis-bipyridyl chiral complexes, which direct the formation of three-dimensional oxalate-based enantiopure families with general formulae: $[Z^{II}(bpy)_3][M_2(ox)_3]$, $[Z^{II}(bpy)_3][X][MM'(ox)_3]$,[38–41] $[Z^{II}(ppy)(bpy)_2][MM'(ox)_3]$[42] and $[Z^{III}(ppy)_2(bpy)][MM'(ox)_3]$[43] ($Z^{II}$ = Fe, Co, Ni, Ru; Z^{III} = Ir; X = ClO_4^-, BF_4^- and PF_6^-; M, M′ = Li^I, Na^I, Mn^{II}, Ni^{II}, Co^{II}, Fe^{II}, Cu^{II}, Zn^{II}, Rh^{III}, Co^{III}, Cr^{III}, Fe^{III}; bpy = 2,2′-dipyridyl, ppy = phenylpyridine). To understand this increase in the dimensionality we must invoke the chirality of the bimetallic network. In fact, while metal centres exhibit alternating chirality in the honeycomb 2D systems, these 3D CPs are composed of homochiral units as a result of the intrinsic D_3 symmetry of the templating complexes which force the $[M^{III}(ox)_3]^{3-}$ building blocks to adopt a homochiral configuration (ΔΔ or ΛΛ; Fig. 2b). From a geometrical point of view, the existence of only one diastereoisomeric building-block avoids the possibility of growing along the plane, forcing the system to grow in three dimensions. From a magnetic point of view, these compounds behave as ferro- and ferrimagnets with lower critical temperatures than their 2D analogues. Taking into account that the magnetic connectivity is mainly the same despite the higher dimensionality, this change can be explained on the basis of the weaker magnetic exchange mediated by the longer metal-to-metal distances and the different relative orientation of the magnetic orbitals.[44]

One step further in the control of the dimensionality of these systems can be accomplished through the use of capping ligands, which can restrict the growth of the bimetallic complexes, yielding for example 1D oxalate-bridged chains[45] or discrete polynuclear complexes such as dimers,[46] trimers[47,48] or tetramers.[49,50] A strict control of the synthesis and solubility of the species in the reaction medium has also permitted the isolation of pure oxalate complexes as dimers or trimers.[51–53]

All these examples outline the vital role of the cation in tailoring the assembly of the molecular building-blocks and therefore controlling the dimensionality of the resulting bimetallic framework. In addition, the substitution of these electronically innocent cations with other electroactive ones can increase the complexity of these systems, conferring novel properties on the final material. This chemical strategy towards the development of hybrid oxalate-based magnetic materials including an additional functionality will be illustrated in the following sections.

Magnetic organic/inorganic heterospin networks

We have been interested in the incorporation of paramagnetic species as non-innocent cations in the synthesis of 2D and 3D oxalate-based networks with the aim of analyzing the synergy between the two magnetic systems. Both the influence of the paramagnetic guest in the ordering parameters of the bimetallic magnet and the effect of the internal magnetic field in the spin polarisation of the guest are subjects of study. In this context, two types of templating spin carriers have been used: decamethylferricinium cations and nitronyl nitroxide (NN) cationic free radicals.[54–57] The main difference between these two families of hybrid organic/inorganic magnets is that, while the spin density of the decamethylferricinium cations is buried between the cyclopentadiene units, NN radicals offer their spin density to the environment interacting with the extended inorganic counterpart. Consequently, in the first family of compounds the two magnetic sub-lattices are completely independent and the paramagnetic cations behave as excellent local probes of the internal field created by the metallic layers. On the other hand, the magnetic properties of the second

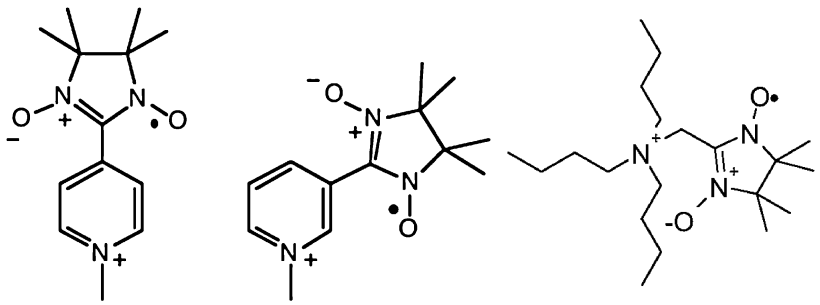

Fig. 3 Structure of the different NN free radicals used in the synthesis of hybrid materials based on bimetallic oxalates. From left to right: *p*-rad, *m*-rad and NN radical of the *N*-alkylpyridinium type.

family of compounds are always indicative of exchange interactions between the organic free radical-based and inorganic sub-lattices. In the following, the review will be restricted to systems incorporating cationic NN free radicals of the *N*-alkylpyridinium and tetraalkylammonium types (Fig. 3).

Magnetic hybrid heterospin networks based on NN free radicals of the *N*-alkylpyridinium type

Since the early reports of Awaga, salts combining cationic NN free radicals of the *N*-alkylpyridinium type with anionic metal complexes have been extensively studied.[58–61] A further step was the use of these cations as bridging units located between oxamate-based bimetallic chains to yield fascinating interlocked structures.[39,62,63] Inspired by these results, we decided to investigate the use of these free radicals as functional cations in the formation of oxalate-bridged extended bimetallic compounds. With the aim of studying the influence of the position of the NN fragment with respect to the pyridine ring, two different *N*-methylpyridinium derivatives bearing a NN moiety in positions 4 (*p*-rad) or 3 (*m*-rad) of the pyridine ring were considered.

2D honeycomb-like oxalate-bridged bimetallic networks with radicals *p*(*m*)-rad located in the interlayer space

Compounds [*p*-rad][$M^{II}Cr(ox)_3$]·nH_2O [M^{II} = Mn, Co, Ni, Zn] and [*m*-rad][$M^{II}Cr(ox)_3$]·nH_2O [M^{II} = Mn, Co] were obtained in moderate yields by adding the cationic free radical to a solution containing $[Cr(ox)_3]^{3-}$ and M^{2+} ions. Using concentrated solutions in a slightly polar solvent, the desired products were recovered by fast precipitation. Under these kinetically controlled conditions, 2D oxalate-based magnets incorporating *p*-rad or *m*-rad in the interlamellar space could be obtained. The 2D nature of these compounds was inferred from their magnetic properties, as shown below. It was observed that the more symmetric *p*-rad cation has a stronger affinity for the 2D honeycomb lattice than *m*-rad, as the yields of the precipitation reactions were higher for the former. It seems that the formation of the hexagonal cavities around the pyridinium cation is partially hindered by the presence of the bulky NN group in the *meta*-position.

The magnetic properties of both Mn(II) derivatives are similar. They order ferromagnetically at 5.7 and 5.3 K and exhibit a soft magnetic behaviour with coercive fields, measured at 2 K, of 66 G and 17 G for the *p*-rad and *m*-rad derivatives, respectively. The value of the critical temperatures, the softness of the materials and the shape of the AC magnetic susceptibility showing a cusp (Fig. 4a) below T_C are the fingerprints of the 2D MnCr lattice. As already observed in other layered oxalate-based materials, the critical temperatures of the Co(II) and Ni(II) compounds are considerably higher with values ranging between 15.5 K for the nickel derivative and 11.3 K for the cobalt one (Table 1). Particularly interesting is the value of the coercive field of [*p*-rad][$CoCr(ox)_3$] (4400 G), which is among the highest reported for 2D bimetallic oxalates and considerably higher (Fig. 4b) than that observed for [*m*-rad][$CoCr(ox)_3$] (230 G).

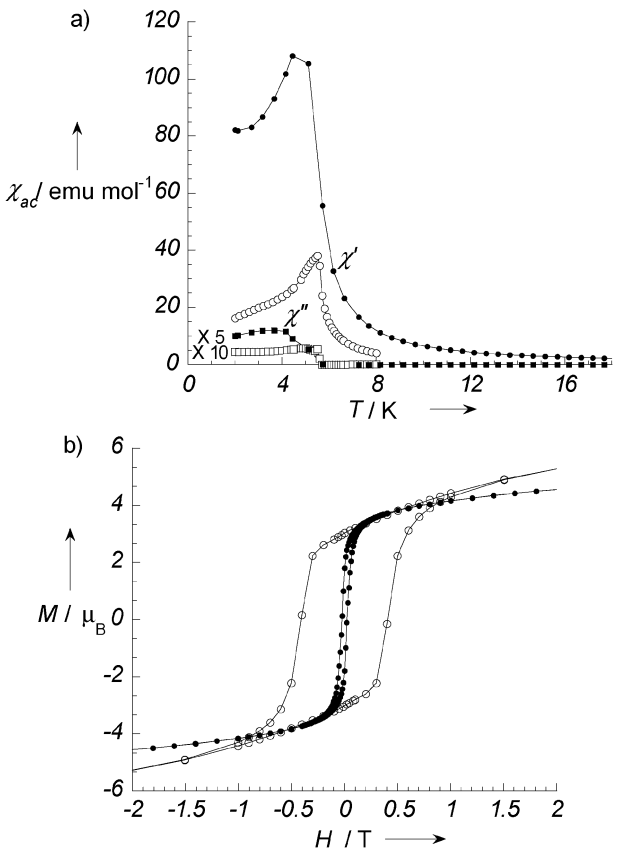

Fig. 4 (a) Temperature dependence of the real and imaginary components of the AC magnetic susceptibility of [*p*-rad][$MnCr(ox)_3$] (empty symbols, operating frequency: 1 Hz) and [*m*-rad][$MnCr(ox)_3$] (filled symbols, operating frequency: 110 Hz); (b) Low-field region of the hysteresis loops of [*p*-rad][$CoCr(ox)_3$] (empty symbols) and [*m*-rad][$CoCr(ox)_3$] (filled symbols) measured at 2 K.

Table 1 Magnetic parameters for the hybrid 2D heterospin compounds [rad][$M^{II}Cr(ox)_3$]

rad$M^{II}M^{III}$	C/emu K mol^{-1}	Θ/K	T_C/K	M_S/μ_B	H_{Coer}/kG
p-radMnCr	6.13	8.0	5.7	7.74	0.066
p-radCoCr	5.37	10.0	13.8	6.22	4.4
p-radNiCr	3.14	17.2	15.5	5.57	1.5
p-radZnCr	2.29	2.8	—	—	—
m-radMnCr	6.55	7.0	5.3	7.37	0.017
m-radCoCr	5.24	11.0	11.3	5.17	0.23
^{n}Bu$_3$NCH$_2$NNMnCr	6.69	7.9	5.7	7.1	0.05
^{n}Bu$_3$NCH$_2$NNNiCr	3.50	28	15.5	5.24	1.34
^{n}Bu$_3$NCH$_2$NNZnCr	2.03	2.4	—	—	—

Definitions: Curie constant (C), Weiss constant (Θ), critical temperature (T_C), saturation magnetization (M_S), and coercive field at 2 K (H_{Coer}).

This huge difference between the *p*-rad and *m*-rad analogues was attributed to the presence of metal defects in the latter, although a particle size effect could not be excluded.

Formation of novel 1D and 3D oxalate-bridged networks induced by the presence of NN free radicals

Under thermodynamic control (using more diluted and aqueous conditions), novel crystalline phases were obtained for the manganese(II)-containing products [*p*-rad][$MnCr(ox)_3(H_2O)$]·$2H_2O$ and [*m*-rad][$MnCr(ox)_3(H_2O)_2$]·$2H_2O$. At this point it is worthwhile recalling that most of the oxalate-bridged extended compounds synthesised as single crystals are Mn(II) derivatives. This is not surprising since, due to the larger size of this cation, the formation of complexes with the $[Cr(ox)_3]^{3-}$ species is weakened and competition between these anions and the water solvent molecules is installed, leading to slower formation of the extended lattice. This competition can result in the coordination of water molecules to the Mn(II) ion, leading to the formation of a wide variety of structures.

The structure of the hybrid salt [*p*-rad][$MnCr(ox)_3(H_2O)$]·$2H_2O$ (monoclinic, C_c space group) shows an achiral 3D oxalate-bridged bimetallic network. It can be described as zig-zag Mn–Cr alternating chains running along the *c* axis, with the Mn(II) and Cr(III) cations being connected by bis-bidentate μ_2-oxalate bridges (Fig. 5). In contrast with the classical 3D network, built up from homochiral building blocks that combine into helical chains, the chirality of the metal centres follows the sequence …ΔΔΛΛΔΔ… along these chains. Two distinct bisbidentate bridges are then found: one connecting metal centres of the same chirality (Mn1···Cr1: 5.421(3) Å) and a second one connecting centres of opposite chirality (Mn1···Cr1: 5.3927(16) Å). These chains are also linked by an uncommon type of oxalate bridge (Fig. 5) that is simultaneously bidentate (towards chromium) and monodentate (towards manganese).[49,64,65] As expected, the metal-to-metal distance (Mn1···Cr1: 5.5977(14) Å) is higher as compared to the bis-bidentate bridging mode. A water molecule occupies the vacant position in the Mn(II) coordination sphere. The linkage between chains results in the formation of an achiral 3-connected decagon network (Fig. 5). The decagonal units are arranged in such a way that helical hexagonal channels are formed. The *p*-rad cations sit in the channels with the N–O functions well separated from each other (the minimum intermolecular O1···O2 distance is 6.891(5) Å). This situation is special in the context of magnetic materials containing nitroxide radicals, where shorter O···O contacts at about 3.5 Å are generally observed.

Regarding its magnetic behaviour, it can be fitted in the paramagnetic regime (Fig. 6) to a regular AB ferromagnetic chain model[66] with classical spins $S_A = 5/2$ and $S_B = 3/2$ ($H_{ex} = -J\sum S_{Ai}S_{Bi}$). The best-fit value for the exchange coupling constant is $J = +0.6$ K. The ferromagnetic character of the Mn^{II}–Cr^{III} magnetic interaction mediated by bis-bidentate oxalate anions is in agreement with previous results. At lower temperatures, the compound exhibits an antiferromagnetic ordering that is driven by weak antiferromagnetic interactions between the chains. These interactions are certainly transmitted through the bidentate/monodentate oxalate anion. The lower symmetry of this bridge decreases the efficiency of the ferromagnetic pathway (as compared to the bis-bidentate ligand) and the antiferromagnetic term becomes dominant, as it has been described for a chromium–manganese tetramer.[49,50] The radicals seem to remain uncoupled to the antiferromagnetically ordered network, a hypothesis that is corroborated by the presence of a Curie tail at low temperatures.

The structure of [*m*-rad][$MnCr(ox)_3(H_2O)$]·$2H_2O$ (triclinic $P\bar{1}$ space group) shows a 1D ladder-like oxalate-bridged bimetallic network. The overall structure is achiral as a result of the presence of an inversion centre that relates the chains (Fig. 7). The steps of the ladder are defined by bis-bidentate oxalate bridges between adjacent $[Cr(ox)_3]^{3-}$ and Mn(II) ions (Mn1···Cr1: 5.4631(7) Å), while the lateral chains are built from bidentate/monodentate bridges that propagate along the *b* axis (Cr1···Mn1: 5.8370(7) Å and Mn1···Cr1: 5.9902(7) Å). This situation leads to two vacant *cis* positions in the Mn(II) coordination sphere, being occupied by water molecules. The free radicals are strongly bonded to the ladders *via* hydrogen bonding (Fig. 7).

The magnetic properties of this system could be analyzed using a spin-ladder chain model with competing interactions: ferromagnetic, in the steps of the ladder, and antiferromagnetic, along the rungs. This yielded a diamagnetic $S = 0$ ground state. The free radicals were considered as an independent paramagnetic contribution, as was the related *p*-rad derivative (*vide supra*). The best-fit data (Fig. 8) for the two magnetic coupling parameters were $J = +0.8$ cm^{-1} and $j = -0.35$ cm^{-1}. As expected, the positive interaction was of the same order of magnitude as that estimated for the *p*-rad analogue.

Magnetic hybrid heterospin networks based on NN free radicals of the tetraalkylammonium type

In the last section we have shown how the fast precipitation of 2D metal–radical hybrid materials result in the formation of amorphous powders. Oppositely, the change of these reaction conditions led to novel oxalate-bridged networks of lower symmetry. With the aim of preparing crystalline 2D materials, we developed the synthesis of tetraalkylammonium NN free radicals. Tetraalkylammonium cations can have a C_3 local

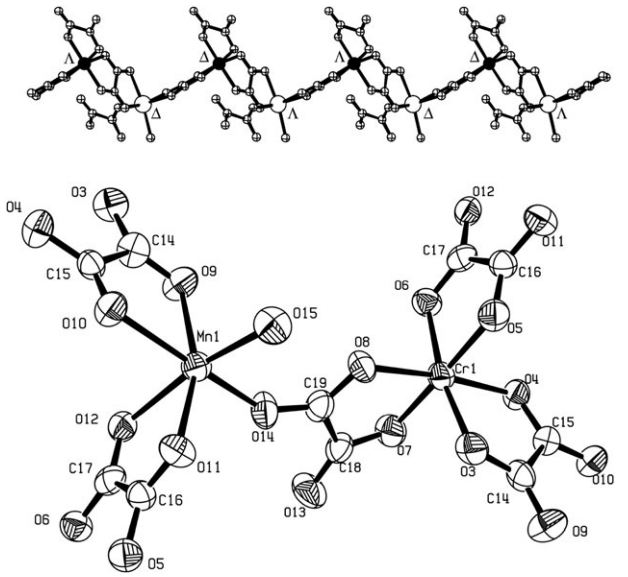

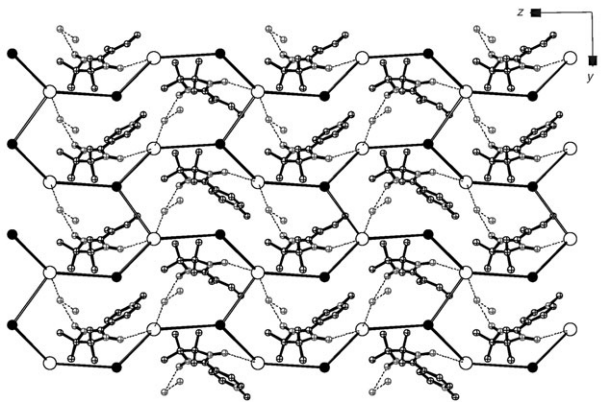

Fig. 5 *Top*: View of the oxalate-bridged MnCr ferromagnetic chains in [*p*-rad][MnCr(ox)$_3$(H$_2$O)] along the *b* axis. The absolute configuration of the metal centres is also shown. *Middle*: Molecular structure of a [Mn(H$_2$O)Cr(ox)$_3$]$^-$ fragment (ellipsoids are set at the 50% probability level; all H atoms have been omitted for clarity). *Bottom*: view of the crystal structure along the *a* axis. Oxalate anions have been replaced by straight rods: black (bis-bidentate) and white (bidentate/monodentate). Dotted lines refer to hydrogen bonds, ○ = Mn, ● = Cr.

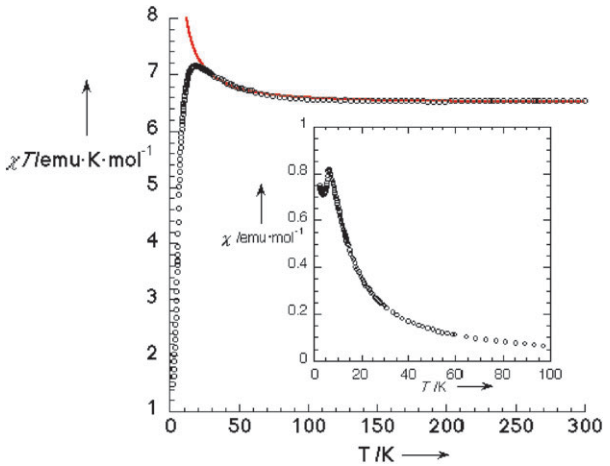

Fig. 6 Thermal variation of the χT product (open circles) for [*p*-rad][MnCr(ox)$_3$(H$_2$O)]. The solid line represents the best-fit data for a ferromagnetic MnCr chain with $J = +0.6$ K. *Inset*: Temperature dependence of χ for the same compound.

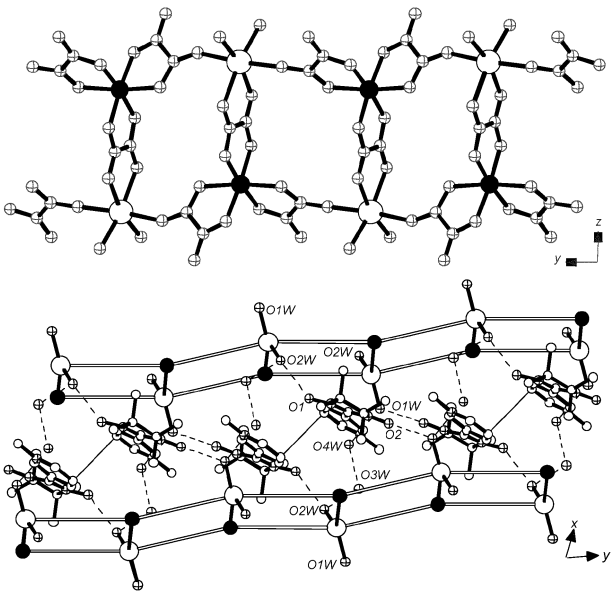

Fig. 7 *Top*: Projection of the crystal structure of [*m*-rad][MnCr(ox)$_3$(H$_2$O)$_2$] onto the *bc* plane, showing the oxalate-bridged MnCr ladder-like chains. *Bottom*: Projection onto the *ab* plane, showing the radical zig-zag chains of dimers and the oxalate-bridged ladder. Oxalate anions have been replaced by straight rods: black (bis-bidentate) and white (bidentate/monodentate). Dotted lines refer to hydrogen bonds, ○ = Mn, ● = Cr.

symmetry similar to that of the hexagonal layers and they combine to form crystalline phases. A cation of this type bearing an appended NN subunit (^{n}Bu$_3$NCH$_2$NN$^+$) could be prepared as a chloride salt by reaction of tributylamine with the radical synthon ClCH$_2$NN.[67] By using this cation, a family of hybrid magnets of formulae [^{n}Bu$_3$NCH$_2$NN][MCr(ox)$_3$] (M = Mn, Ni, Zn) could be isolated.

The crystal structure of the Mn(II) derivative contains the well-known honeycomb lattice. The interlayer spacing (half of the *c* parameter in the *P*6$_3$ space group) is 8.905(2) Å, very similar to that previously reported for a tetrabutylammonium analogue.[33] Between the layers, the cationic free radical ^{n}Bu$_3$NCH$_2$NN$^+$ is severely disordered due to site symmetry (three-fold axis) and also to conformational disorder of the butyl chains. As in previously reported crystal structures containing a bimetallic oxalate network and ^{n}Bu$_4$N$^+$ cations, one of the butyl fragments penetrates into the hexagonal cavities. Thus, the free radical moiety should be located in the interlayer space in any of the three equivalent positions created by the ternary axis.

The magnetic properties of these systems are those expected for the layered systems. The Mn(II) derivative behaves as a soft ferromagnet with $T_C = 5.7$ K and $H_C = 50$ G (at 2 K), while the Ni(II) analogue orders ferromagnetically at $T_C = 15.5$ K and has a coercive field of 1340 G at 2 K. As expected, the Zn(II) compound is paramagnetic, but a close look at its

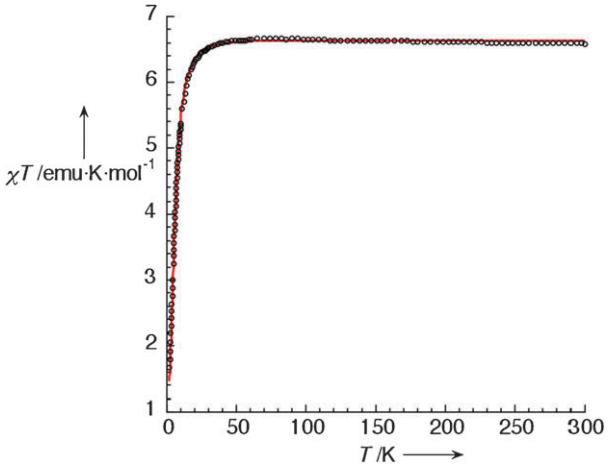

Fig. 8 Thermal variation of the χT product (open circles) for [*m*-rad][$MnCr(ox)_3(H_2O)_2$]. The solid line represents the best-fit data ($J = +0.8$ cm^{-1}; $j = 0.35$ cm^{-1}).

low temperature behaviour reveals the presence of weak ferromagnetic interactions that take place probably between the free radicals and the $[Cr(ox)_3]^{3-}$ anions. These interactions were also detected by EPR (electronic paramagnetic resonance) spectroscopy.

The EPR spectrum at high temperature of the Mn–Cr system (Fig. 9) shows a single line centred at $g = 2.021$ with a peak-to-peak width $\Delta H_{pp} = 320$ G. The asymmetric signal of the Cr(III) moiety and the characteristic peak of the free radical are not observed. At low temperatures this feature splits into two lines that show opposite shifts. This behaviour can be explained if we assume that this slightly anisotropic feature originates from the sum of the parallel ($g_{\|}$) and perpendicular ($g_{\perp}$) components of the nitroxide radical. Thus, at low temperatures the onset of magnetic ordering creates an internal magnetic field that adds (or subtracts) to the external applied magnetic field, resulting in a shift of the nitroxide radical signal towards lower (or higher) fields. These shifts can be clearly seen in the plot of the signal position as a function of temperature. Note that the signal starts to split around 20 K, well above the critical temperature, signalling the presence of short-range interactions inside the layers. When lowering the temperature, the correlation length increases along with the internal field. At the lower temperature measured (4.2 K) the internal field is about 4000 G for both signals, close to the value observed in the $[FeCp^*_2][MnCr(ox)_3]$ compound[54,55] and higher than that observed (1500 G) in hybrid systems derived from *p*-rad cations. These features parallel the previously reported data for $[FeCp^*_2][MnCr(ox)_3]$. In this case, however, the free radical does not show an intrinsic signal, indicating exchange interactions between the two magnetic sub-lattices.

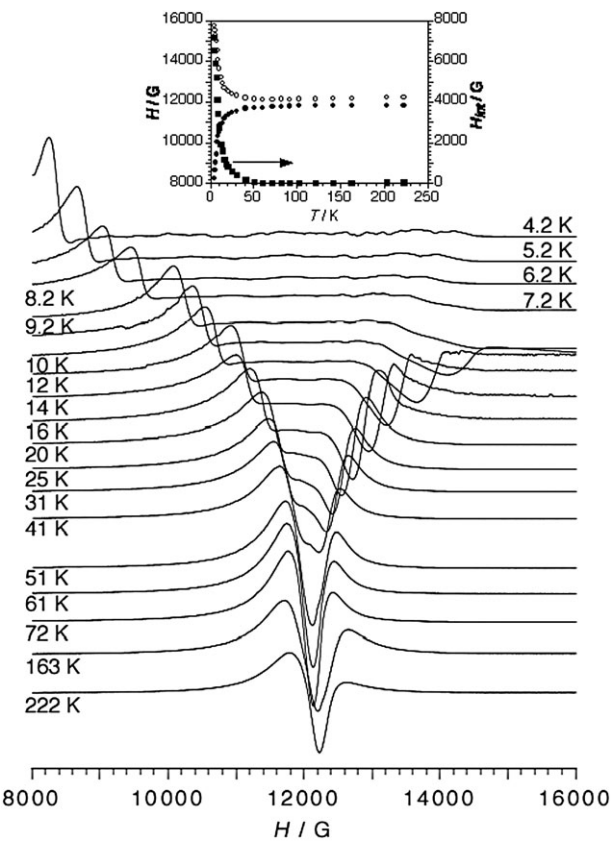

Fig. 9 EPR spectra (Q-band) of [^{n}Bu$_3$NCH$_2$NN][$MnCr(ox)_3$] at different temperatures. The inset shows the thermal dependence of the positions of the peaks of the signals and the internal field.

In this section, the ability of cationic free radicals of the nitronyl nitroxide type to act as countercations of extended oxalate-bridged bimetallic compounds has been demonstrated. In this way, hybrid materials that combine nitroxide free radicals and ferromagnetic layers, with similar magnetic properties that those previously observed in the quaternary ammonium analogues $[AR_4][MCr(ox)_3]$ (A = N, P), could be obtained. In the case of NN free radicals derived from *N*-alkylpyridinium cation, it was possible to direct the synthesis in such a way that the hybrid 2D magnets were obtained under kinetic control, whereas working under thermodynamic control afforded new heterodimetallic oxalate-based lattices that result from partial occupation of the vacant positions of the divalent metal by water molecules. We have shown that the size and shape of the free radical determines the geometry and dimensionality of these novel hybrid materials: whilst *p*-rad stabilizes a 3D achiral network of hellicoidal hexagonal channels, *m*-rad acts as countercation of a ladder-like anionic structure. The influence of the free radical in the structure of the inorganic host is possible by the existence of hydrogen bonds that involve adventitious solvent molecules.

In the layered multifunctional hybrid magnets, the paramagnetic cation has little influence on the ordering temperatures but it has a marked effect on the coercive field values, although this effect can be correlated with other features such as the particle size. The most significant feature of this family of hybrid radical-based magnets is the presence of a sizeable interaction between the free radicals and the inorganic layers.

Finally, we have also demonstrated the efficiency of paramagnetic nitronyl nitroxide cationic free radicals, based on tetraalkylammonium salts with local C_3 symmetry, as templates for the growth of 2D hexagonal oxalate-based layered ferromagnets.

Hybrid magnetic materials formed by bimetallic oxalato complexes and spin-crossover molecules

Spin crossover (SCO) complexes are particularly suitable for the preparation of multifunctional magnetic materials since they represent one of the best examples of magnetic bi-stability at the molecular level.[68,69] Among them, those charged positively, pave the way for the design of switching magnets in which the magnetic ordering of the bimetallic anionic oxalate framework might be tuned through the external modulation of the SCO phenomenon, as triggered by light or pressure. In addition, the internal pressure created by the magnetic framework might affect the spin-crossover properties of the inserted SCO molecule. So far, several examples have described the incorporation of SCO complexes into oxalate-based networks. Whilst the first ones were solely restricted to Co(II) and Fe(II) complexes, a larger variety of compounds have been recently obtained with Fe(III) complexes of the hexadentate Schiff base ligand, sal_2-trien (H_2sal_2-trien = *N*,*N*′-disalicylidenetriethylene-tetramine) and derivatives (Fig. 10).

In 2000, Decurtins *et al.* reported the first example of the insertion of SCO cations into oxalate networks. $[Co(bpy)_3][LiCr(ox)_3]$ is a polymetallic salt exhibiting a 3D chiral structure, with the high-spin (HS) $[Co^{II}(bpy)_3]^{2+}$ (bpy = 2,2′-bipyridine; $C_{10}H_8N_2$) complexes occupying the internal cavities offered by the oxalate-bridged framework.[70] Interestingly, the size of these holes was found to determine the spin state of the incorporated SCO complex. This was exemplified by the $[Co(bpy)_3][NaCr(ox)_3]$ derivative, where the substitution of Na^+ with Li^+ reduced the size of the cavity. This structural change increases the chemical pressure suffered by the SCO complex to such an extent, that the low-spin (LS) state became the most favourable energetically. Unfortunately, the paramagnetic nature of the oxalate network in these compounds prevented the coexistence of SCO and magnetic ordering.

More recently, in 2007, Sato and co-workers used the SCO complex $[Co^{II}(terpy)_2]^{2+}$ (terpy = 2,6-bis(2-pyridyl)pyridine; $C_{15}H_{11}N_3$) to grow $[Co(terpy)_2][Mn(H_2O)ClCr(ox)_3]\cdot H_2O\cdot 0.5CH_3OH$ 1D chains, and 2D layered compounds with formula $[Co(terpy)_2][Mn(H_2O)Cr(ox)_3]_2\cdot 5H_2O\cdot 0.5CH_3OH$.[71] The first is composed of bimetallic anionic chains, which contain alternating $[Mn(H_2O)Cl]^+$ and $[Cr(ox)_3]^{3-}$ units interconnected through two bis-bidentate chelating oxalate linkers belonging to the latter. On the other hand, the 2D system, which is isolated in the absence of Cl^- anions, is formed by alternating layers of the SCO cations and the anionic oxalate-bridged layer with formula $[Mn(H_2O)Cr(ox)_3]_n^{n-}$. Across each layer, the Cr(III) centres are octahedrally connected to three bis-bidentate oxalate dianions, whilst the Mn (units) exhibit a completely different situation with its coordination sphere being occupied by two bis-bidentate oxalate ligands, one monodentate and a coordinating water molecule. This atypical coordination mode for the oxalate linker has already been described in the previous section. On the basis of their static magnetic susceptibility, both compounds exhibit ferromagnetic interactions but no signature of long-range magnetic ordering was detected above 2 K. Besides, the intrinsic SCO of the Co(II) complex is again suppressed by the chemical pressure imposed by the metal–organic framework.

In a further step, we have exploited this same strategy to incorporate a Fe(II) SCO complex, $[Fe(bpp)_2]^{2+}$ (bpp = 2,6(bis(pyrazol-3-yl)pyridine; $C_{22}H_{18}N_{10}$), into a bimetallic oxalate-based network (Fig. 10). $[Fe(bpp)_2][MnCr(ox)_3]\cdot(bpp)\cdot(CH_3OH)$ represents a novel type of achiral 3D oxalate-based network, which is composed of metal centres exhibiting both chiralities in sharp contrast with the more common enantiopure chiral structures described for the family of oxalate-based 3D architectures.[72] Hence, in this atypical example, homochiral and heterochiral pairs of metal centres linked through the oxalate ligand coexist in the same structure. Regarding its magnetic properties, this system behaves as a soft ferromagnet below 3 K but no clear SCO transition is observed.

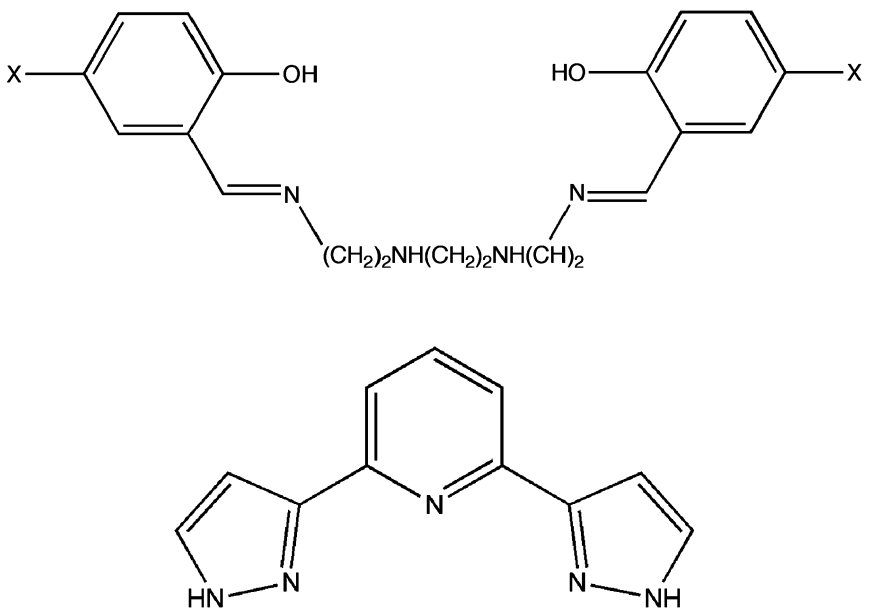

Fig. 10 Structure of the $H_2$5-Xsal_2-trien (X = H, NO_2, Cl, CH_3O, CF_3O, Cl, Br; *top*) and bpp (*bottom*) ligands

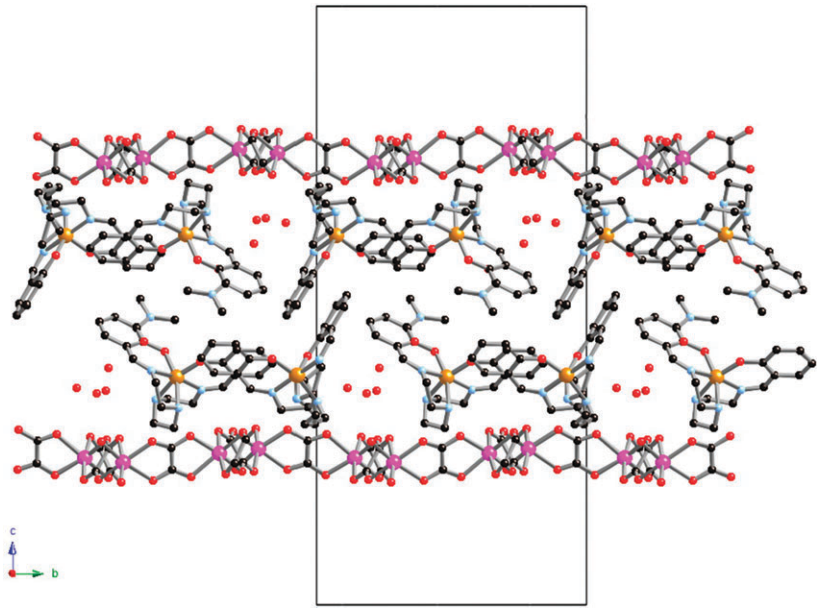

Fig. 11 Lateral view of the anionic and cationic layers of $[Fe^{III}(sal_2\text{-trien})]_2[Mn^{II}_2(ox)_3]\cdot 4(H_2O)\cdot(C_3H_7NO)$ in the *bc* plane. Fe: yellow; Mn: pink; C: black; N: blue; O: red. Hydrogen atoms have been omitted for clarity.

The coexistence of SCO and magnetic ordering has been very recently achieved in the compound $[Fe^{III}(sal_2\text{-trien})]_2[Mn^{II}_2(ox)_3]\cdot 4(H_2O)\cdot(C_3H_7NO)$.[73] From a structural point of view, this hybrid compound is formed by homometallic Mn(II) oxalate layers, which resemble the classical honeycomb-like 2D motif, with a bi-layer of interleaved $[Fe(sal_2\text{-trien})]^+$ SCO cations (Fig. 11). It is worthwhile to remark that this bi-layer is necessary to counterbalance the negative charge born by the anionic network $[Mn^{II}_2(ox)_3]^{2-}$. This compound behaves as a weak ferromagnet with T_C = 8.1 K, exhibiting at the same time a gradual spin crossover of half of the intercalated $[Fe(sal_2\text{-trien})]^+$ complexes from 300 down to 80 K (Fig. 13; empty squares). Nevertheless, although these two phenomena coexist in the same compound, they remain mainly independent since the change in the spin state of the $[Fe(sal_2\text{-trien})]^+$ guest cations after desolvation does not cause drastic changes in the intrinsic magnetism of the homometallic oxalate-supported host. A significant advance in this context has been provided through the synthesis of the compound $[Fe^{III}(sal_2\text{-trien})][Mn^{II}Cr^{III}(ox)_3]\cdot(CH_2Cl_2)$.[74] It is formed by $[Fe^{III}(sal_2\text{-trien})]^+$ cations intercalated between the honeycomb-like bimetallic layers (Fig. 12). In contrast to the homometallic derivative described above, just a single layer of $[Fe(sal_2\text{-trien})]^+$ cations is intercalated between the oxalate-bridged anionic layers due to the −1 charge supported by the $[Mn^{II}Cr^{III}(ox)_3]^-$ periodic unit. The magnetic properties indicate the coexistence of a complete spin crossover from 300 to 160 K, and a ferromagnetic ordering below 5.4 K (Fig. 13; full circles).

At this point it is interesting to describe how slight variations on the synthetic conditions also permit the stabilization of a three-dimensional structure incorporating the SCO $[Fe^{III}(sal_2\text{-trien})]^+$ complex in the solid-state. $[Fe^{III}(sal_2\text{-trien})][Mn^{II}Cr^{III}(ox)_3]\cdot(CH_3OH)$ can be described as a 3D achiral network equivalent to the $[Fe(bpp)_2][MnCr(ox)_3]\cdot(bpp)\cdot(CH_3OH)$ system (*vide supra*) but incorporating different SCO units (Fig. 14). This system shows a gradual and incomplete spin-crossover of 30% of the Fe(III) centres from 300 to 130 K, together with the ferromagnetic ordering of the 3D lattice below 5.2 K (Fig. 15). The stabilization of two oxalate architectures with different dimensionalities by using the same templating cation is likely due to the structural flexibility of the $[Fe^{III}(sal_2\text{-trien})]^+$

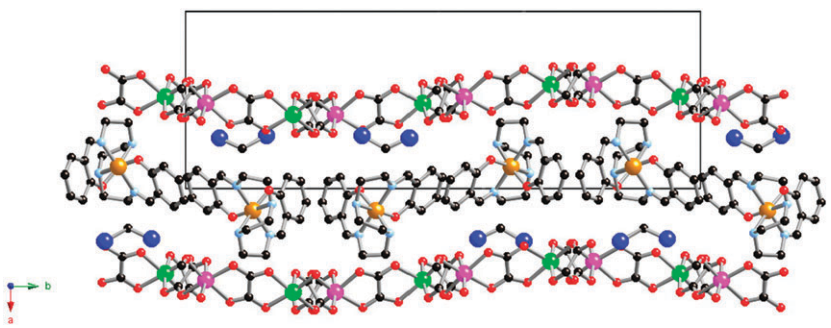

Fig. 12 Lateral view of the cationic and anionic layers of $[Fe^{III}(sal_2\text{-trien})][Mn^{II}Cr^{III}(ox)_3]\cdot(CH_2Cl_2)$ in the *ab* plane. Fe: yellow; Mn: pink; Cr: dark blue; C: black; N: blue; O: red; Cl: green. Hydrogen atoms have been omitted for clarity.

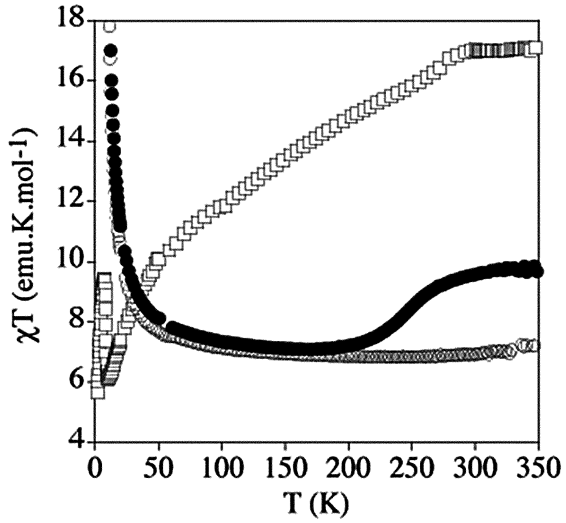

Fig. 13 Temperature dependence of the product of the molar magnetic susceptibility with the temperature (χT) at 1000 G for the 2D layered compounds: $[Fe^{III}(5\text{-}NO_2sal_2\text{-}trien)][Mn^{II}Cr^{III}(ox)_3]\cdot(CH_3NO_2)\cdot 0.5(H_2O)$ (empty circles), $[Fe^{III}(sal_2\text{-}trien)][Mn^{II}Cr^{III}(ox)_3]\cdot(CH_2Cl_2)$ (full circles) and $[Fe^{III}(sal_2\text{-}trien)]_2[Mn^{II}{}_2(ox)_3]\cdot 4(H_2O)\cdot(C_3H_7NO)$ (empty squares).

complex. In fact, the relative orientation of the two phenoxy arms of this complex differs notably in different compounds,[75] suggesting that a different configuration of these rings may cause a different templating effect on the assembly of the oxalate network. This seems to be confirmed by the different configurations exhibited by the $[Fe(sal_2\text{-}trien)]^+$ cations in these compounds, with very different values for their dihedral angles, α, defined as the angle formed by the least squares planes of the two phenoxy rings. Whilst in the 2D case this value is clearly smaller than the ideal value for an octahedral complex (90°), the two crystallographically independent $[Fe(sal_2\text{-}trien)]^+$ cations exhibit the opposite behaviour in the 3D framework, with α being larger than 90°. The different mixture of solvents used to dissolve the $[Fe(sal_2\text{-}trien)]^+$ cations in each particular case appears as a plausible explanation for this structural change.[74]

By exploiting this synthetic strategy, we have been able to isolate related magnetic frameworks incorporating other derivatives of the $[Fe^{III}(sal_2\text{-}trien)]^+$ complex with different substituents at position 5 of the salicylaldimine ring. Among them, the $[Fe^{III}(5\text{-}NO_2sal_2\text{-}trien)]^+$ complex, in which the presence of NO_2 groups favours π–π stacking interactions, gives rise to a 2D network with formula $[Fe^{III}(5\text{-}NO_2sal_2\text{-}trien)][Mn^{II}Cr^{III}(ox)_3]\cdot(CH_3NO_2)\cdot 0.5(H_2O)$, whilst the $[Fe^{III}(5\text{-}CH_3Osal_2\text{-}trien)]^+$ derivative, in which the steric hindrance introduced by the methoxy groups makes these supramolecular interactions less favourable, directs the formation of the achiral 3D network $[Fe^{III}(5\text{-}CH_3Osal_2\text{-}trien)][Mn^{II}Cr^{III}(ox)_3]$.[76] In contrast to the structural flexibility encountered when using the non-substituted $[Fe^{III}(sal_2\text{-}trien)]^+$ complex, in the present examples only one type of structure is obtained for each cation independently of the synthetic conditions used.

Regarding their overall structure, the $[Fe^{III}(5\text{-}NO_2sal_2\text{-}trien)][Mn^{II}Cr^{III}(ox)_3]\cdot(CH_3NO_2)\cdot 0.5(H_2O)$ two-dimensional phase is rather different to the 2D structure obtained with the non-substituted $[Fe(sal_2\text{-}trien)]^+$ cation. Thus, it crystallizes in the chiral space group $P2_1$ and within each anionic layer, all the Cr(III) ions adopt a homochiral configuration (Δ), whereas all the Mn(II) centres adopt the opposite configuration (Λ), following a …ΔΛΔΛ… pattern. Besides, according to the chiral space group, the configuration of each metal ion is preserved in the neighbouring oxalate layers. Since the synthesis was carried out from a racemic mixture of the $[Cr(ox)_3]^{3-}$ (Δ and Λ), the isolated material is composed of crystals of both enantiomers. A similar behaviour has been observed in other 2D oxalate-based structures.[77,78] The intrinsic chirality of the $[Fe^{III}(5\text{-}NO_2sal_2\text{-}trien)]^+$ cations may be responsible for this

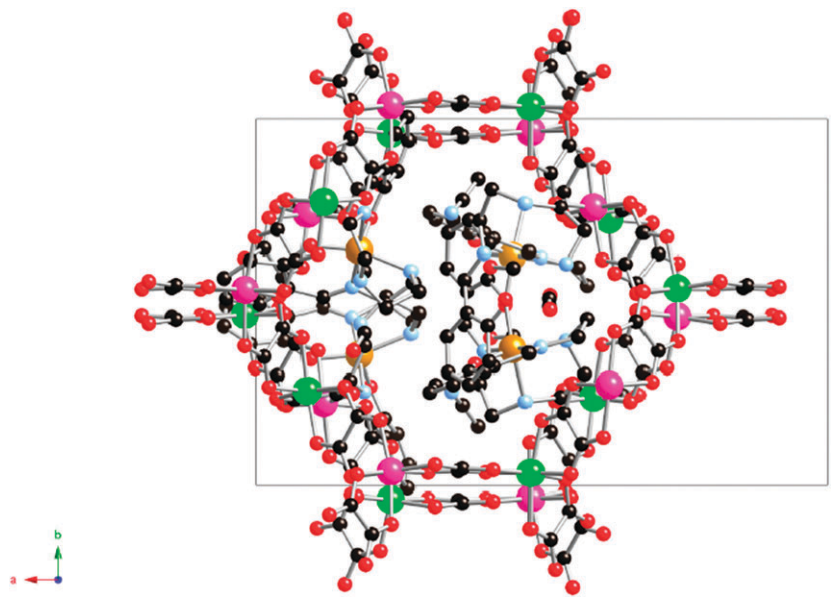

Fig. 14 Projection of $[Fe^{III}(sal_2\text{-}trien)][Mn^{II}Cr^{III}(ox)_3]\cdot(CH_3OH)$ in the *ab* plane. Fe: yellow; Mn: pink; Cr: green; C: black; N: blue; O: red. Hydrogen atoms have been omitted for clarity. Only one of the two configurations of the disordered $[Fe^{III}(5\text{-}CH_3O\ sal_2\text{-}trien)]^+$ molecule is shown for clarity.

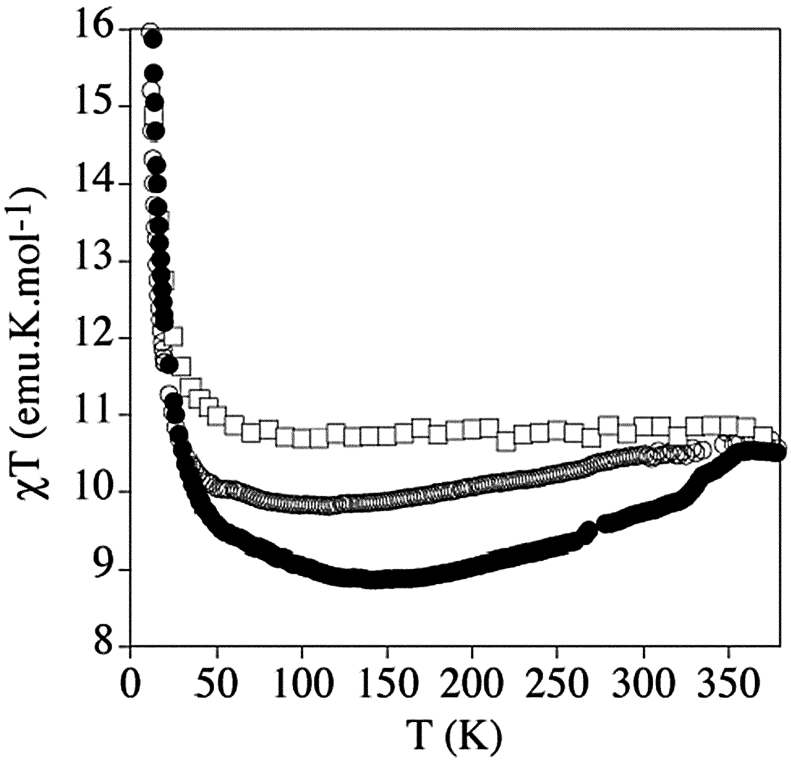

Fig. 15 Temperature dependence of the product of the molar magnetic susceptibility with the temperature at 1000 G for the 3D derivatives: $[Fe^{III}(sal_2\text{-trien})][Mn^{II}Cr^{III}(ox)_3]\cdot(CH_3OH)$ (empty circles), $[Fe^{III}(5\text{-}CF_3Osal_2\text{-trien})][Mn^{II}Cr^{III}(ox)_3]\cdot 0.5(CH_3OH)$ (full circles) and $[Fe^{III}(5\text{-}CH_3Osal_2\text{-trien})][Mn^{II}Cr^{III}(ox)_3]$ (empty squares).

first-order spontaneous resolution through chiral recognition between one of the enantiomers of $[Cr(ox)_3]^{3-}$ and the Fe(III) complex. This homochiral configuration of the metal sites within a given layer is not observed in the $[Fe^{III}(sal_2\text{-trien})]$-$[Mn^{II}Cr^{III}(ox)_3]\cdot(CH_2Cl_2)$ compound, in which the metal ions exhibit both configurations. Besides, in the $-NO_2$ derivative, the extended bimetallic network, built up from the interconnection of metal centres and bis-bidentate oxalate linkers, forms an almost perfect honeycomb-like lattice, in contrast with the undulation of the oxalate-supported layer observed in

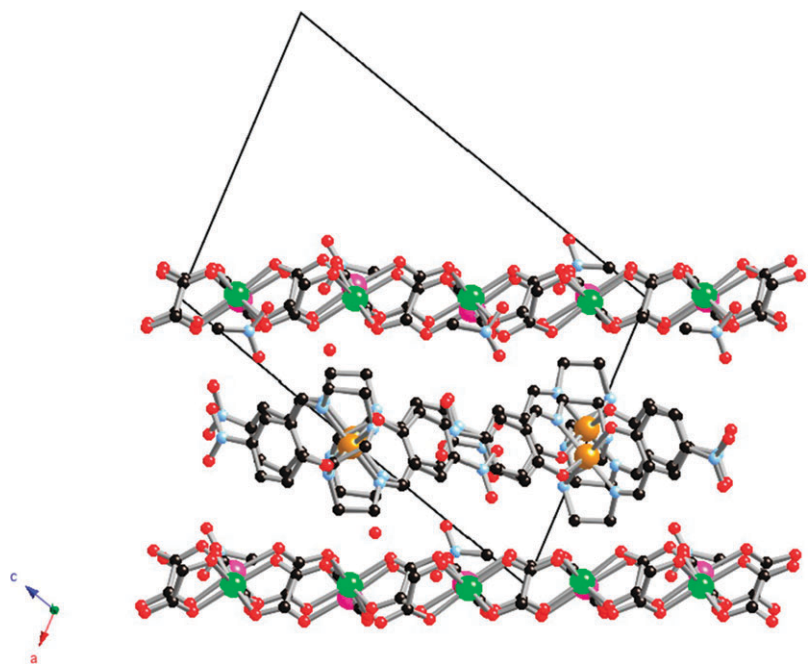

Fig. 16 Lateral view of the anionic and cationic layers of $[Fe^{III}(5\text{-}NO_2sal_2\text{-trien})][Mn^{II}Cr^{III}(ox)_3]\cdot(CH_3NO_2)\cdot 0.5(H_2O)$ projected in the −101 plane. Fe: yellow; Cr: green; Mn: pink; C: black; N: blue; O: red. Hydrogen atoms have been omitted for clarity.

the non-substituted sal-trien derivative (Fig. 16). Concerning the oxalate network of the achiral 3D compound, $[Fe^{III}(5\text{-}CH_3Osal_2\text{-}trien)][Mn^{II}Cr^{III}(ox)_3]$, it is equivalent to that of its 3D counterparts obtained with $[Fe^{II}(bpp)_2]^{2+}$ and $[Fe^{III}(sal_2\text{-}trien)]^{+}$ (*vide supra*).

On the basis of their magnetic properties, both the 2D and the 3D materials undergo long-range ferromagnetic ordering at *ca.* 5 K. On the other hand, the inserted Fe^{III} cations remain mainly in the LS state in the case of the 2D compound, $[Fe^{III}(5\text{-}NO_2sal_2\text{-}trien)][Mn^{II}Cr^{III}(ox)_3]\cdot(CH_3NO_2)\cdot0.5(H_2O)$, and in the HS state in the case of the 3D compound, $[Fe^{III}(5\text{-}CH_3Osal_2\text{-}trien)][Mn^{II}Cr^{III}(ox)_3]$ (Fig. 13 and 15). These results demonstrate that the electronic state of the SCO guest can be effectively tuned by controlling the electron-withdrawing or electron-donating character of the substituent in the sal_2-trien periphery. In this way, the electron-withdrawing substituent $-NO_2$, favours the LS state whereas the electron-donating group CH_3O-, favours the HS one. This chemical control of the inserted cation's spin state with the substituent can also be observed in the family of compounds with a very similar achiral 3D network as illustrated by the comparison between $[Fe^{III}(5\text{-}CH_3Osal_2\text{-}trien)][Mn^{II}Cr^{III}(ox)_3]$ and $[Fe^{III}(sal_2\text{-}trien)][Mn^{II}Cr^{III}(ox)_3]\cdot(CH_3OH)$, described above, and $[Fe^{III}(5\text{-}CF_3Osal_2\text{-}trien)][Mn^{II}Cr^{III}(ox)_3]\cdot0.5(CH_3OH)$, which has been also obtained.[79] In this family, the derivative bearing the electron-donating group CH_3O- remains in the HS state over the whole range of temperatures whilst the compounds containing less electron donating groups, H– and CF_3O-, show a gradual spin-crossover transition of 30 and 50% of the inserted Fe(III) metal centres, respectively, as the system is cooled down (Fig. 15).

We are currently exploring the preparation of related compounds by introducing other organic substituents in the positions 5 (Cl, Br), 3 and 4 (CH_3O, Cl and Br) of the salicylaldimine ring. Our preliminary results show a great variety of structures ranging from different 2D phases for the 3 and 4 substituted derivatives to a 3D chiral network, $[Fe^{III}(5\text{-}Xsal_2\text{-}trien)][Mn^{II}Cr^{III}(ox)_3]$ (X = Cl and Br), when position 5 is derivatized (Fig. 17).[79]

This section has illustrated how multifunctional magnetic materials, combining long-range magnetic ordering and spin crossover, can be obtained using a hybrid approach. This new class of materials represent an avenue for the preparation of an advanced generation of switchable magnetic materials. The following step is to tune the SCO phenomenon, introduced by the cationic guest, by applying external stimuli. This has already been illustrated in two layered oxalate-based architectures: (a) the hometallic $[Fe^{III}(sal_2\text{-}trien)]_2[Mn^{II}_2(ox)_3]\cdot4(H_2O)\cdot(C_3H_7NO)$, which exhibits a gradual SCO transition that is suppressed by the desolvation of the cationic complex and (b) the bimetallic $[Fe^{III}(sal_2\text{-}trien)][Mn^{II}Cr^{III}(ox)_3]\cdot(CH_2Cl_2)$, whose SCO transition can be tuned under light irradiation. In this latter example, the conversion from the LS to HS state induced by light-irradiation, commonly known as the LIESST effect (light-induced excited spin-state trapping), has been achieved.[80] This effect has been widely described for Fe(II) complexes but it is very unusual for Fe(III) complexes, for which only two examples have been reported so far.[81–83] This different behaviour is likely due to the mechanism of the LIESST effect. Hence, in Fe(III) complexes the relaxation *via* a tunnelling process between the photo-generated metastable HS state and the LS ground state is much faster than in Fe(II) compounds because the changes in the metal-to-ligand bond lengths between the two states are significantly smaller for Fe(III) complexes.[84]

Unfortunately, in these examples the change in the spin-state in the molecular complexes does not efficiently modify the magnetic behaviour of the extended two-dimensional

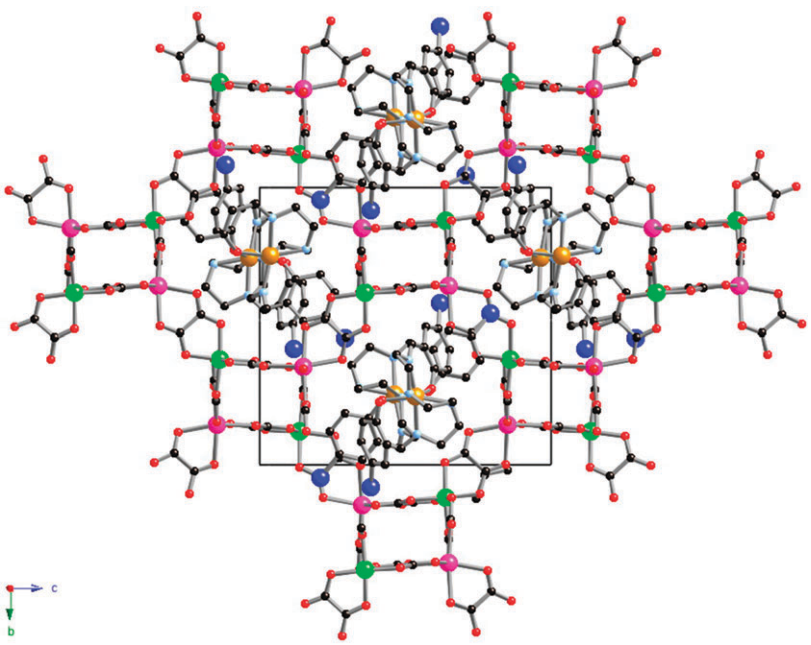

Fig. 17 Projection of $([Fe^{III}(5\text{-}Clsal_2\text{-}trien)][Mn^{II}Cr^{III}(ox)_3]$ in the *bc* plane. Fe: yellow; Mn: pink; Cr: dark blue; C: black; N: blue; O: red; Cl: green. Hydrogen atoms have been omitted for clarity.

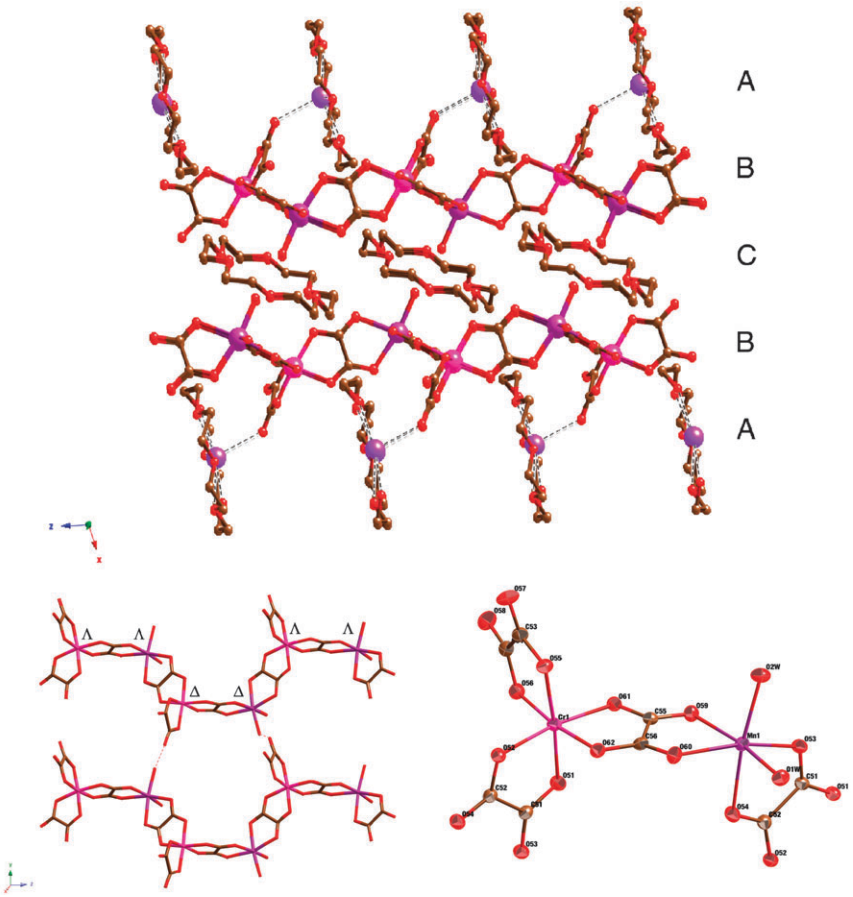

Fig. 18 Projection of the crystal structure of [K-(18-crown-6)][$Mn(H_2O)_2Cr(ox)_3$] on the *ac* plane showing the alternating layers along the *a* axis (*top*). View of the {[$Mn(H_2O)_2Cr(ox)_3$]}$^-$ chains showing the hydrogen-bonded network in the anionic layers (*bottom left*). Thermal ellipsoid representation (50% probability) of the octahedral coordination of Cr^{3+} and Mn^{2+} metal centres (*bottom right*). Cr: pink; Mn: purple; K: magenta; C: brown; O: red. Hydrogen atoms have been omitted for clarity.

oxalate-bridged networks. The lack of interaction between the two phenomena in both solids is not surprising and must be attributed to the intrinsic nature of this family of 2D oxalate-based layered magnets. In fact, due to their two-dimensional nature, these layered compounds do not exhibit significant changes in their T_C values for different interlayer separations. To solve this point and design an efficient switching magnet, the 3D bimetallic framework has been shown to be more appropriate in view of its higher sensitivity to the influence of internal pressure.[43]

Finally, the discovery that the [$Fe(sal_2$-trien)]$^+$ complexes can present LIESST effects is very interesting from a fundamental point of view since the appearance of this effect in Fe(III) SCO complexes is quite unusual. It is tempting to attribute such a behaviour to the influence of the bimetallic oxalate network on the SCO guest. If that is so, the chemical approach here presented could be a suitable strategy to induce the appearance of LIESST effects in other Fe(III) cations, or even to improve the LIESST properties in this type of complex.

Soluble magnets

All the examples reported above have illustrated how the shape, size and charge of the cations are key elements for the preparation of different oxalate-based architectures. Still, in all these cases the resulting hybrid solid has proved to be insoluble in water and other polar solvents. In view of that, we attempted to use crown ether-based complexes as templating cations, as for example [K-(18-crown-6)]$^+$. Two reasons justified this choice: (a) its planar shape could result in the formation of unprecedented magnetic topologies and (b) the presence of oxygen atoms in its structure, may facilitate the formation of hydrogen bonds, therefore introducing supramolecular interactions that should be important in tailoring the final assembling of the molecular entities in the framework, whilst at the same time enabling these CPs to be dissolved in water.

Using the [K(18-crown-6)]$^+$ cation in the formation of novel oxalate-bridged magnetic architectures: initial steps

The first successful example in this direction was the isolation of the ferromagnetic oxalate-based chain: [K-(18-crown-6)][$Mn(H_2O)_2Cr(ox)_3$].[85] This system was isolated by using as a template the cation [K(18-crown-6)]$^+$, in the presence of an excess of neutral 18-crown-6 ether molecules. It is soluble in water and insoluble in organic solvents, and can only be isolated under particular synthetic conditions as an insoluble product therefore suggesting its kinetic nature.

From a structural point of view, this compound is composed of three alternating layers, which are formed respectively by $[K(18\text{-crown-6})]^+$ cationic molecules (A), $[Mn(H_2O)Cr(ox)_3]^-$ anionic chains (B) and neutral 18-crown-6 molecules (C), packed following a ...BCBA... pattern (Fig. 18). These bimetallic chains are built up from $[Cr(ox)_3]^{3-}$ complexes covalently bonded to Mn(II) ions through bis-bidentate chelating oxalate bridges. Whilst the divalent ions are octahedrally surrounded by two chelating oxalate ligands and two coordinating water molecules, the Cr(III) atoms are connected to two bridging and one terminal oxalate ligand. These chains are formed from both enantiomers of the corresponding octahedral metallic complexes, but instead of following the typical zig-zag alternating arrangement, the complexes appear as pairs of identical chirality following the sequence ...ΛΛΔΔ... (Fig. 18) As displayed in Fig. 19, one water molecule bound to the Mn(II) centre is pointing towards the neutral crown ether molecule whereas the other interacts with the neighbouring chain through a hydrogen bond (O···O 2.176 Å) with an oxygen atom belonging to the neighbouring terminal oxalate. The rest of the oxalate terminal ligands are oriented towards the cationic $[K(18\text{-crown-6})]^+$ complexes probably due to the electrostatic interaction between the potassium atom, located within the crown cavity, and one of the oxygen atoms belonging to the organic ligands (O···K 2.654 Å). This interaction also determines the pseudo-hexagonal packing of the crown ether complexes in the cationic layer. Each neutral layer is sandwiched by two anionic layers in such a way that oxygen atoms from the 18-crown-6 ether molecules show some hydrogen bonding contacts with two water molecules from the adjacent anionic layers, one above and one below (O···O 2.778 and 2.879 Å).

From a magnetic point of view, this compound behaves as a soft ferromagnet below 3.5 K due to the combination of the ferromagnetic exchange through the oxalate bridges operating along the chain and the weaker ferromagnetic inter-chain interactions introduced by the hydrogen bonding interactions connecting the chains (Fig. 20). In this context, it is worthwhile remarking that H-bonding interactions have already demonstrated their ability to effectively transmit magnetic interactions in other molecule-based magnets.[86]

An entire family of 2D water-soluble layered magnets

Small modifications in the synthetic procedure have permitted an increase in the dimensionality of this sort of compound leading to the synthesis of a family of 2D layered magnets with general formula $[K(18\text{-crown-6})]_3[M^{II}{}_3(H_2O)_4\{M^{III}(ox)_3\}_3]$ (M^{III} = Cr, Fe; M^{II} = Mn, Fe, Ni, Co, Cu).[87,88] These compounds can be prepared by the dropwise addition of a methanolic solution containing the M(II) ions to the corresponding $[K(18\text{-crown-6})]_3[M^{III}(ox)_3]$ complexes also dissolved in methanol and, as already mentioned for the 1D polymer above, can be solubilised in water. This feature facilitates the production of large, good quality single crystals under specific conditions as illustrated in Fig. 21.

These bimetallic salts are isostructural and crystallize in the monoclinic $C2/c$ space group. They are composed of alternating cationic ($[K\text{-}(18\text{-crown-6})]^+$, (A)) and anionic ($[M^{II}{}_3(H_2O)_4\{M^{III}(ox)_3\}_3]^-$, (B)) layers following a ...ABAB... pattern (Fig. 22). This anionic polymeric network is reminiscent of the classical honeycomb-like structural motif previously described by Okawa *et al.*[30] but, in this case, the connectivity is broken by the presence of water molecules in the divalent ion coordination sphere, forcing a fraction of the oxalate groups to act as terminal ligands, thus resulting in the existence of two different types of M^{2+} and M^{3+} metallic centres. In this way, M^{2+} centres can be divided into $M^{2+}(1)$ and $M^{2+}(2)$ ions in a 2 : 1 ratio, with $M^{2+}(1)$ ions being surrounded by two bis-bidentate chelating oxalate ligands and two coordinating water molecules in an octahedral geometry and $M^{2+}(2)$ centres being only coordinated to chelating oxalate ligands. Accordingly, two different $[M^{III}(ox)_3]^{3-}$ units can be observed in the same ratio, with one of them being connected to three M^{2+} ions through bis-chelating oxalate bridges and the other connected to two M^{2+} ions through chelating oxalate ligands and one M^{2+} ion *via* the hydrogen-bonding interaction between terminal oxalate ligand and the neighbouring coordinating water molecules (O···O 2.588 and 2.634 Å; Fig. 23). This fact leads to an increase in the metal-to-metal distance to increase from the 5.43–5.45 Å range, typical for a bis-chelating oxalate bridge, to 7.77 Å. The consequences of this structural feature on the magnetic properties of this family of compounds will be described later.

In each layer all M^{3+} ions are homochiral and have opposite chirality to that of the M^{2+} metallic centres. The layers show

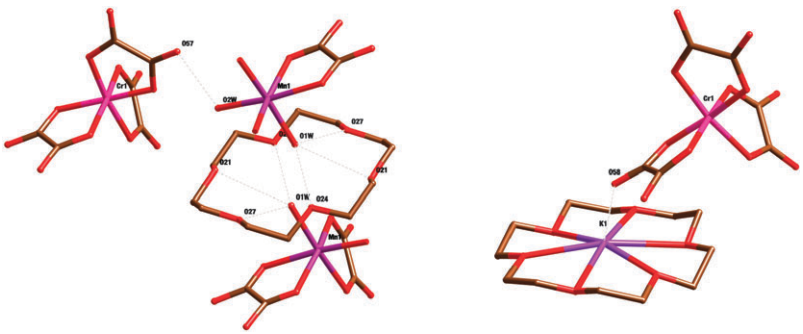

Fig. 19 Picture depicting the hydrogen bonding interactions between the anionic network and the neutral crown ether molecule in $[K\text{-}(18\text{-crown-6})][Mn(H_2O)_2Cr(ox)_3]$ (*left*). Electrostatic interactions between the terminal oxalate ligand bonded to the Cr^{3+} ion and the potassium ion encapsulated within the crown ether molecule (*right*).

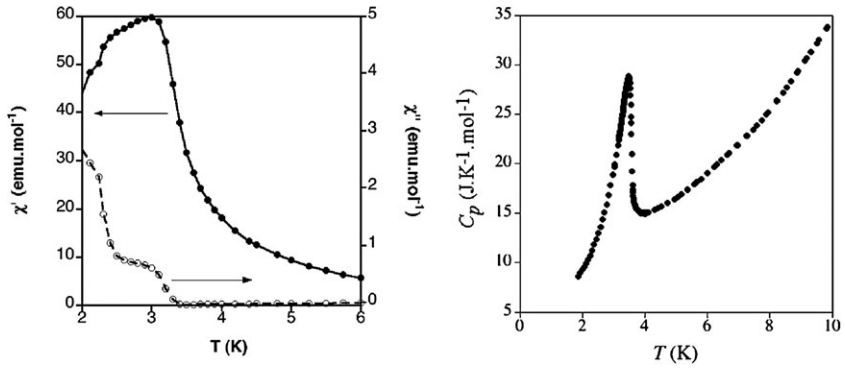

Fig. 20 AC susceptibility at 332 Hz for $\{[K\text{-}(18\text{-crown-}6)][Mn(H_2O)_2Cr(ox)_3]\}_\infty$ (*left*). In-phase susceptibility is represented by filled symbols whereas out-of-phase susceptibility is represented by empty ones. Heat capacity measurements showing the appearance of a lambda peak related to the onset of magnetic ordering (*right*). Solid lines are only a guide to the eye.

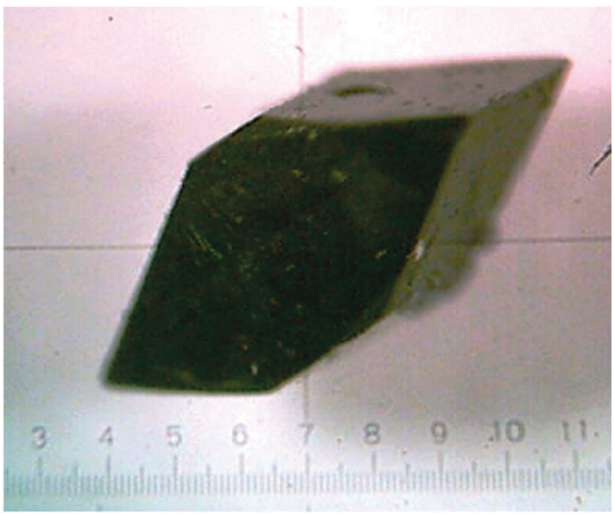

Fig. 21 Single crystal of $[K\text{-}(18\text{-crown-}6)][Mn_3(H_2O)_4\{Cr(ox)_3\}_3]$ obtained by slow diffusion of its components in a mixture of water and methanol.

eclipsed packing, with adjacent layers possessing opposite chiralities and orientations as they are related by a centre of symmetry. If only coordination bonds are considered, the structure is formed by 14-membered rings, with alternating M^{2+} and M^{3+} centres of opposite chirality. Otherwise, if the H-bonding are also taken into account, the structure presents 6-membered rings of two types: one type with five oxalate and one H-bonded oxalate bridges and the other one with two H-bonding interactions. This causes an elongation of the diagonal of the hexagon from $\sim$10.8 Å, for a perfect honeycomb-like structure, to 12.29 and 14.60 Å, respectively. Overall, the oxalate-bridged layer resembles a precursor of the well-known 2D hexagonal network. Actually, if the coordinated water molecules were eliminated and the corresponding H-bonded oxalate ligands took their place as chelating moieties, the result would be the formation of the classical honeycomb-like structure.

Regarding the cationic layers, they are composed of a pseudo-hexagonal packing of $[K\text{-}(18\text{-crown-}6)]^+$ complexes. Again, the presence of electrostatic (O···K 3.104 and 3.180 Å) and hydrogen-bonding (O···O 2.712 and 2.738 Å) interactions between the crown ether complex and the terminal oxalate ligand belonging to the adjacent anionic layer seems to affect their packing in the solid-state. This way, they are oriented essentially perpendicular to the *c* axis, with the mean plane of the crown ether ring forming an angle of approximately 26° with respect to the anionic network, defining an interlayer separation of 8.18 Å. This value, defined as the distance separating the mean planes of adjacent anionic layers, is in the same range of those reported for related oxalate-based 2D layered magnets.

Another structural characteristic of this sort of compounds resides in the displacement of the cationic crown ether complexes with respect to the central position of the hexagonal channels, as defined by the packing of the bimetallic anionic oxalate-based network along the *c* axis. This contrasts with that observed in other families of honeycomb-like layered materials like the $[M^{II}Cp^*_2][M^{II}M^{III}(ox)_3]$ series,[54] where the organometallic cations exhibit a staggered conformation and are located in the central position of the hexagonal channels. Such a difference is likely caused by the larger diameter of the $[K\text{-}(18\text{-crown-}6)]^+$ complex with respect to the $[M^{II}Cp^*_2]^+$ organometallic cation, 9.2 *vs.* 8.0 Å, which promotes the network fragmentation as a consequence of the larger volume of the moiety to be located in the interlayer space (Fig. 24). In fact, the complex size was estimated from the length of the symmetry axis perpendicular to that of maximum symmetry. To prove this hypothesis, we attempted to introduce the smaller 15-crown-5 ether molecule in the bimetallic lattice and succeeded in the isolation of the $[K\text{-}(15\text{-crown-}5)_2][MnCr(ox)_3]$ layered system (Fig. 25).[89] As expected, in this case the classical honeycomb layer $[MnCr(ox)_3]^-$ is formed with the cationic layers of $[K\text{-}(15\text{-crown-}5)_2]^+$ complexes located in the central position of the hexagonal channels as result of electrostatic interactions with its neighbouring oxygen atoms (O···O from 2.888 to 3.235 Å).

From a magnetic point of view these compounds follow the general trend observed for other bimetallic oxalate-based architectures, with the Cr(III) derivatives exhibiting ferromagnetic ordering between 3 and 8 K and the Fe(III)-based compounds presenting ferrimagnetic behaviour between 12 and 26 K, except for the Mn(II) case, which behaves as a weak ferromagnet below 14 K due to spin canting between

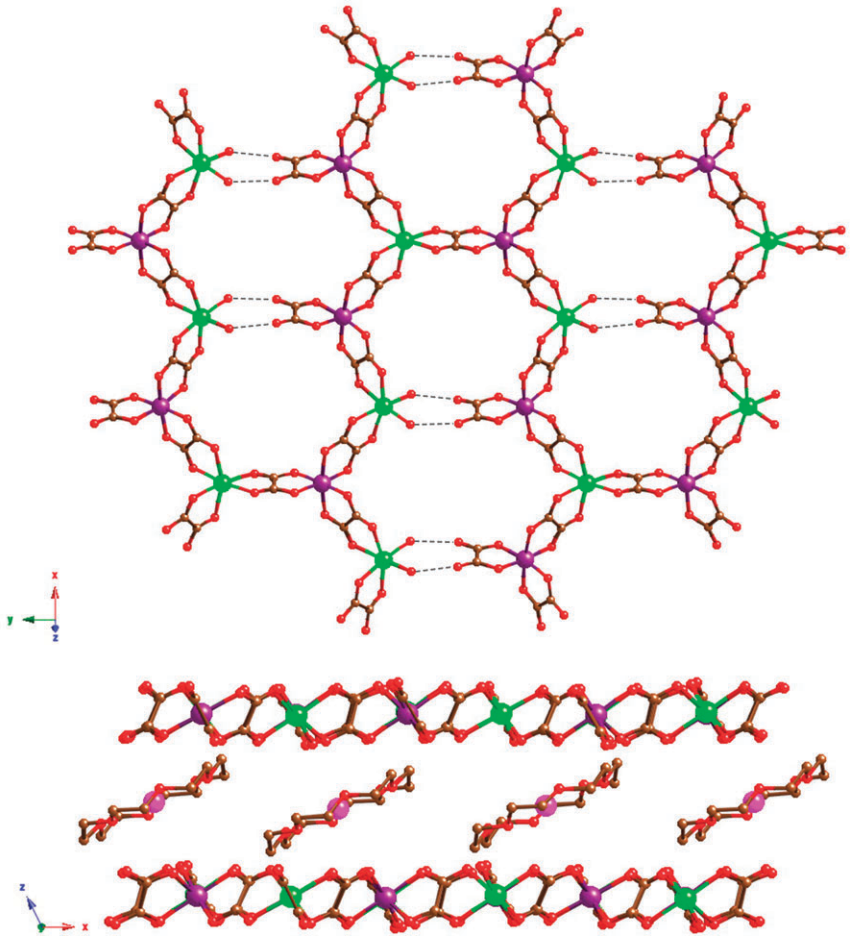

Fig. 22 Perspective showing the pseudo-hexagonal configuration of the 2D fragmented anionic polymeric network in the family $[K(18\text{-crown-6})]_3[M^{II}{}_3(H_2O)_4\{M^{III}(ox)_3\}_3]$ (M^{III} = Cr, Fe; M^{II} = Mn, Fe, Ni, Co, Cu) (*top*). View of the layered nature of the oxalate-based compound in the solid state (*bottom*). Cr: purple; Mn: green; K: pink; C: brown; O: red. Hydrogen atoms have been omitted for clarity. H-bonding interactions are represented as dashed bonds.

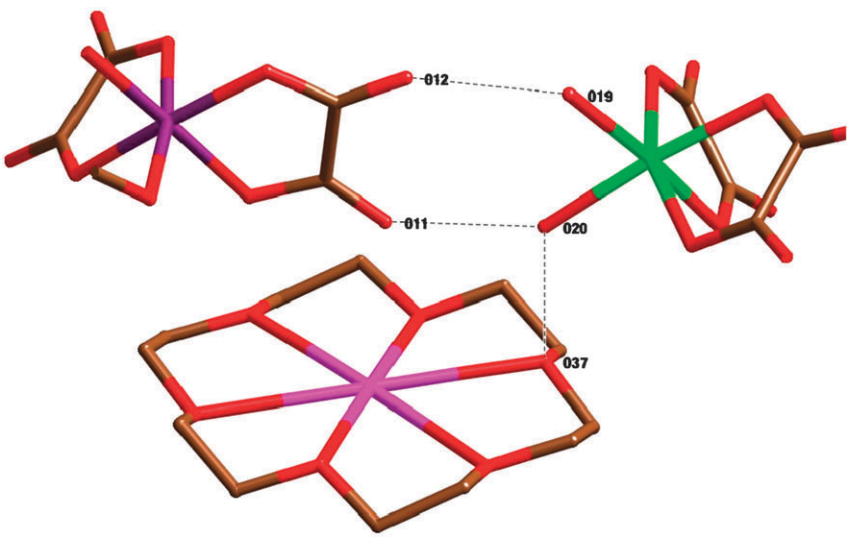

Fig. 23 Hydrogen bonding interactions (dashed bonds) across the anionic network and between the crown ether cationic complex and the coordinating water molecules belonging to the oxalate-based framework.

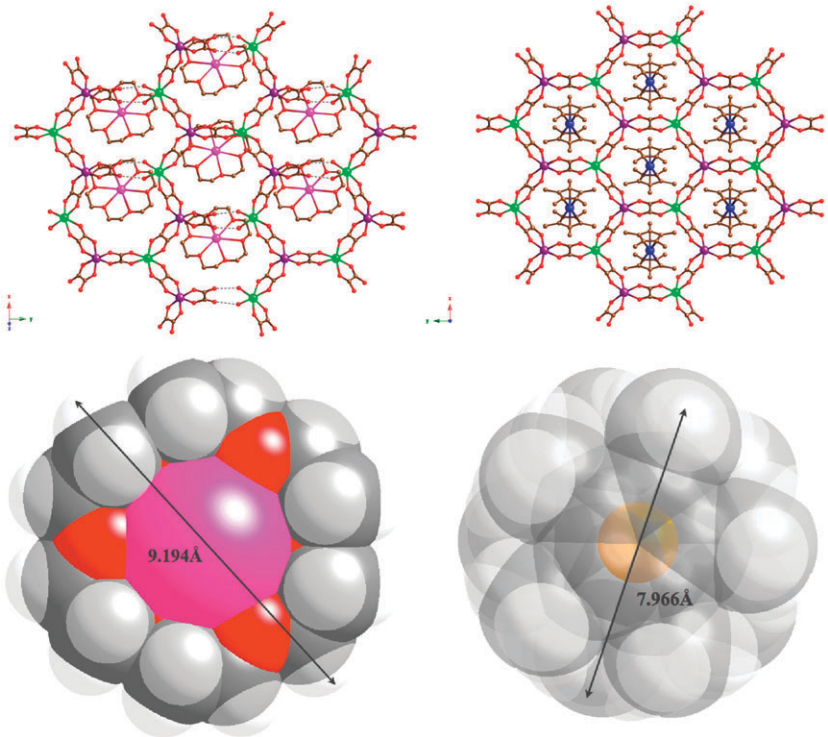

Fig. 24 Top: perspective showing the relative orientation of the cationic complexes ($[K(18\text{-crown-6})]^+$ and $[FeCp^*_2]^+$) with respect to the oxalate-based 2D framework for $[K(18\text{-crown-6})]_3[M^{II}_3(H_2O)_4\{M^{III}(ox)_3\}_3]$ (*left*) and $[FeCp^*_2][MnCr(ox)_3]$ (*right*). Bottom: bulky space representation of the cationic complexes $[K(18\text{-crown-6})]^+$ (*left*) and $[FeCp^*_2]^+$ (*right*), confirming the bigger size of the crown ether based compound as estimated from the length of the axis perpendicular to that of higher symmetry.

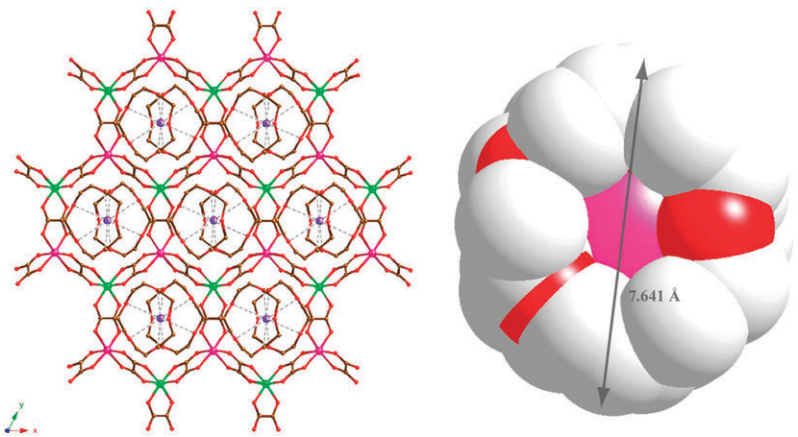

Fig. 25 Perspective showing the structure of $[K\text{-}(15\text{-crown-}5)_2][MnCr(ox)_3]$ along the *ab* plane and the alignment of the $[K\text{-}(15\text{-crown-}5_2]^+$ sandwich-like complexes across the hexagonal channels (*left*). Bulky representation of the $[K\text{-}(15\text{-crown-}5)_2]^+$ complex (*right*).

the two antiferromagnetically coupled magnetic sub-lattices (See Fig. 26 and Table 2). Due to the lower connectivity of the metals across these quasi-2D frameworks, these systems exhibit smaller T_C values than the classical $[XR_4][M^{II}M^{III}(ox)_3]$ 2D honeycomb layered magnets, whose critical temperatures range from 6 K up to 12 K for the Cr(III) derivatives and from 28 to 45 K for the Fe(III) analogues.[30] As described above, in these systems two thirds of the bis-bidentate M^{II}-ox-M^{III} oxalate bridges have been substituted with M^{II}-H_2O–ox–M^{III} hydrogen bonding interactions, therefore decreasing the number of effective exchange pathways within the 2D magnetic framework.

'Cation-less' 2D layered magnets: a vehicle for the nanostructuration of magnetic oxides

All the examples described until now share one common aspect: the extended oxalate-bridged metal–organic framework results from the self-assembly in solution of the anionic low-dimensional oligomeric species with a templating cationic complex, thus producing cation/anion or host/guest bimetallic salts. These examples have proved the importance of supramolecular hydrogen bonding interactions in determining the structure and properties of the resulting material. In fact, despite their weaker strength and lower directionality, this

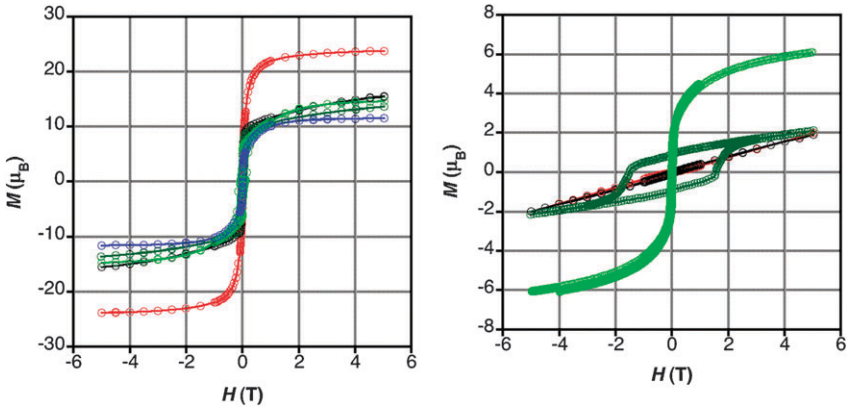

Fig. 26 Hysteresis loops at 2 K for the Cr(III; left) and Fe(III; right) series. Solid lines are only a guide to the eye.

Table 2 Main magnetic parameters for the family $[K(18\text{-crown-6})]_3[M^{II}_3(H_2O)_4\{M^{III}(ox)_3\}_3]$ (M^{III} = Cr, Fe; M^{II} = Mn, Fe, Ni, Co, Cu)

$M^{III}M^{II}$	C/emu K mol^{-1}	Θ/K	T_C/K	M_S/μ_B	M_R/μ_B	H_{Coer}/kG
CrMn	16.39	2.23	3.5	23.90	<0.01	—
CrFe	14.08	11.17	8	15.55	2.32	0.13
CrCo	16.13	2.21	6	13.66	3.69	0.17
CrNi	9.27	21.91	4.5	14.63	4.50	0.79
CrCu	6.66	9.61	3.2	11.58	<0.01	—
FeMn	26.72	−71.32	14	2.01	1.14	0.18
FeFe	24.30	−80.02	25.5	1.93	<0.01	—
FeCo	20.29	−49.68	16	2.13	0.95	15.3
FeNi	17.64	−64.77	11.5	6.64	<0.01	0.23

Definitions: Curie constant (C), Weiss constant (Θ), critical temperature (T_C), saturation magnetization (M_S), remnant magnetization at 2 K (M_R) and coercive field at 2 K (H_{Coer}). $S(Cr^{3+}) = 3/2$, $S(Fe^{3+}) = 5/2$, $S(Mn^{2+}) = 5/2$, $S(Fe^{2+}) = 3/2$, $S(Co^{2+}) = 3/2$, $S(Ni^{2+}) = 1$, $S(Cu^{2+}) = 1/2$.

sort of interaction has already been employed as an effective intermolecular bonding force in the design of purely organic magnets.[58,90] Inspired by this work, we explored the possibility of eliminating the cation in the design and isolation of novel hybrid metal–organic oxalate-based magnetic frameworks.

Our first step in this direction led to the isolation of a family of 'cation-less' oxalate-based 2D polymetallic networks: $[M^{II}(H_2O)_2]_3[M^{III}(ox)_3]_2(18\text{-crown-6})_2$ (M^{III} = Cr, Fe; M^{II} = Mn, Fe, Co, Ni).[91,92] These systems constitute the first example in which the extended metal–organic network framework is intrinsically neutral and does not require the presence of a templating cation for its assembly. Instead, the hydrogen bonding interactions operating between the neutral crown ether molecule and the neighbouring metallic layers seem to be sufficient to stabilize the bimetallic 2D network. As already mentioned, the introduction of 18-crown-6 molecules makes these systems soluble in water whereas they remain non-soluble in other organic solvents. The possibilities that might derive from this unusual property in this particular case will be briefly described in the last part of this section.

These compounds can be isolated by adding an excess of the neutral crown ether molecule to a methanolic solution containing a combination of the M(II) metal cations and the corresponding $[M^{III}(ox)_3]^{3-}$ complex in a stochiometric ratio. They crystallize in the $Pc2_1n$ orthorhombic space group and are composed of neutral bimetallic oxalate-bridged layers of $[M^{II}(H_2O)_2]_3[M^{III}(ox)_3]_2$, defining holes across the layers which are occupied by the 18-crown-6 guest molecules (Fig. 27). These layers are formed by 12-membered rings, constituted of six $[M^{III}(ox)_3]^{3-}$ units and six M(II) atoms, and are perpendicularly oriented with respect to the *ac* plane. Across the layers, each M(III) atom is shared between three rings, whilst the M(II) units are shared between two neighbouring rings. In these rings, each M(II) ion is connected to two bridging bis-bidentate oxalate ligands, belonging to two $[M^{III}(ox)_3]^{3-}$ units, and two coordinating water molecules. From these structural features, two different types of M^{2+} ions, $M^{2+}(1)$ and $M^{2+}(2)$, can be observed a 2 : 1 ratio. Whilst in $M^{2+}(1)$ the two water molecules appear in a *cis* conformation, in $M^{2+}(2)$ they exhibit a *trans* configuration. Each $[M^{III}(ox)_3]^{3-}$ is linked to two $M^{2+}(2)$ and one $M^{2+}(1)$ centres. Regarding the chirality of the tris-oxalate metalate complexes across the layers, they exhibit alternating chirality following a $\ldots M^{2+}(2)\Lambda\Delta\Lambda\Delta\Lambda\Delta M^{2+}(2)\ldots$ pattern with non-chiral $M^{2+}(2)$ ions connecting two M(III) metal centres with opposite chirality.

As already mentioned, the hydrogen bonding interactions play a key role in the isolation of this family of compounds. Hence, the two crown ether molecules located in the middle of each 12-membered ring interact with the bonded water molecules through their oxygen atoms (Fig. 27). While the $O_w\cdots O_{Crown}$ distances for the water molecules coordinated in a *cis* fashion are in the 2.701(2)–3.043(2) Å range, this parameter oscillates between 2.692(2) and 2.979(2) Å for the *trans* molecules. Finally, the absence of interlamellar cations induces an interlayer distance of 7.825(2) Å. This value is significantly smaller than those described for the classical cation-templated 2D phases which range between 8.19 and 14.52 Å for the cations $[N(n\text{-}C_3H_7)_4]^+$ and $[(C_6H_5)_3PNP(C_6H_5)_3]^+$, respectively.[34]

From a magnetic point of view, the layered materials containing $[Cr(ox)_3]^{3-}$ complexes behave as ferromagnets with critical temperatures up to 8 K whereas the $[Fe(ox)_3]^{3-}$ series present ferrimagnetic ordering up to 12 K (See Fig. 28 and Table 3). In this context it is worthwhile mentioning a related compound, the $\{[Mn(OH_2)(CH_3OH)][Mn(OH_2)_2]_2[Cr(ox)_3]_2\text{-}(18\text{-crown-6})\}\cdot CH_3OH$ derivative.[93] This system, which can only be isolated under specific synthetic circumstances, exhibits almost the same overall structure described for this family of compounds except for a particularity: whilst in the

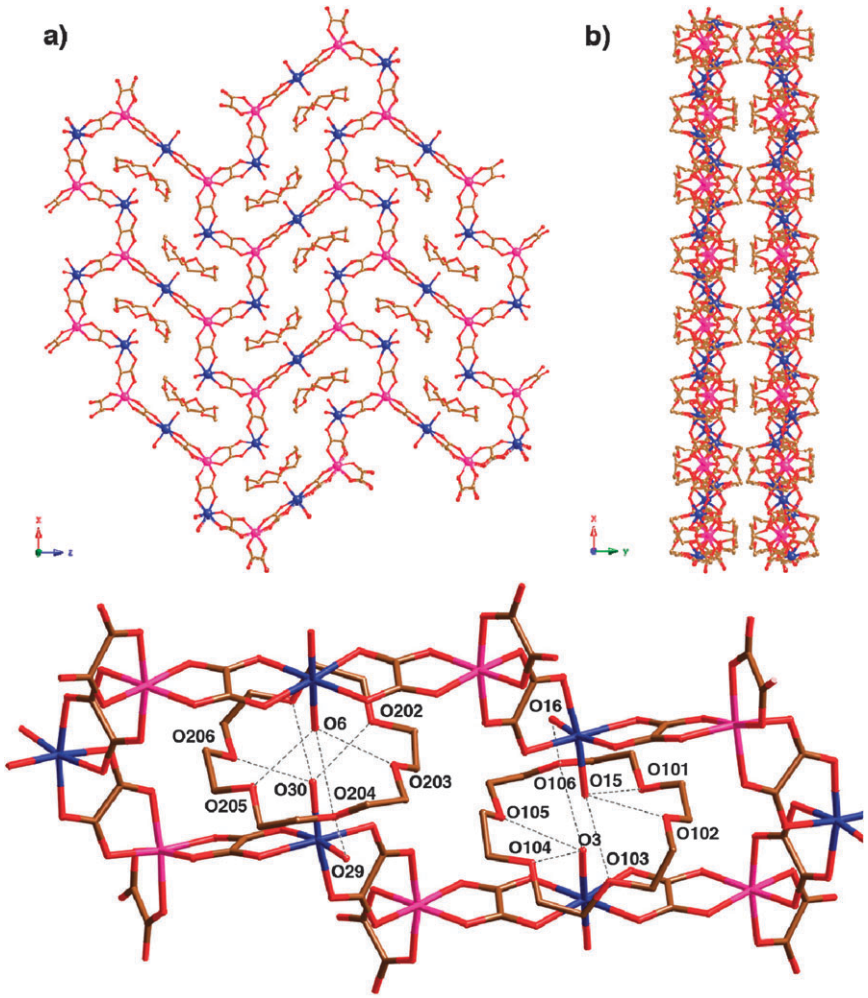

Fig. 27 Top: perspective showing the structure of the neutral polymeric layers in the family $[M^{II}(H_2O)_2]_3[M^{III}(ox)_3]_2(18\text{-crown-}6)_2$ (M^{III} = Cr, Fe; M^{II} = Mn, Fe, Co, Ni) (a), and the packing of these layers along the *b* axis (b). Bottom: hydrogen bonding interactions (dashed bonds) between the 2D oxalate-based framework and the crown ether molecules located in the holes. Cr (pink), Co (blue), O (red) and C (black). Hydrogen atoms have been omitted for the sake of simplicity.

$[M^{II}(H_2O)_2]_3[M^{III}(ox)_3]_2(18\text{-crown-}6)_2$ family the oxalate ligand exhibits the typical bis-bidentate coordinating form, in this particular case two different oxalate bridges—bis-bidentate and bidentate-monodentate—coexist (Fig. 29). This atypical coordination mode[57,64] (see previous sections) has drastic consequences on the magnetism of this system, which exhibits ferrimagnetic ordering above 5.5 K as a result of the combination of two different super-exchange interactions: (a) ferromagnetic through the bis-bidentate oxalate bridge and (b) antiferromagnetic through the bidentate-monodentate one.

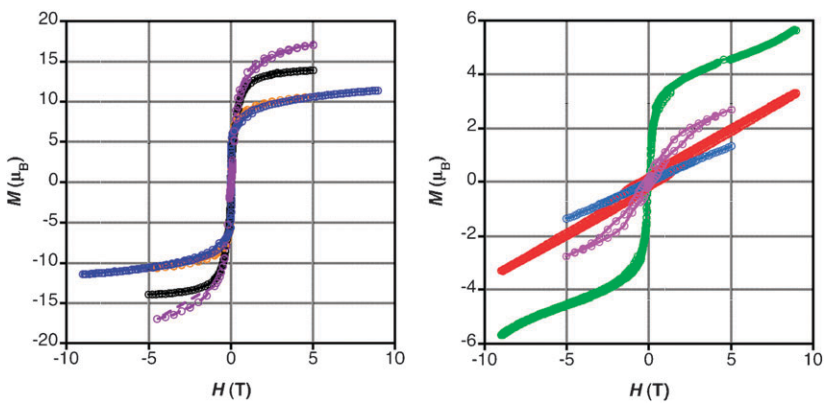

Fig. 28 Hysteresis loops at 2 K for the Cr(III; left) and Fe(III; right) series. Solid lines are only a guide to the eye.

Table 3 Main magnetic parameters for the family $[M^{II}(H_2O)_2]_3[M^{III}(ox)_3]_2(18\text{-crown-}6)_2$ (M^{III} = Cr, Fe; M^{II} = Mn, Fe, Co, Ni)

$M^{III}M^{II}M^{II\prime}$	χT_{rt}	C	C_{SO}	Θ/K	T_C/K	M_S/μ_B	M_R/μ_B	H_{Coer}/kG
CrCoCo	11.8	10.9	9.38	22.6	7.6	11.4	2.3	0.16
CrMnMn	16.4	16.0	16.88	6.6	3.6	17.0	<0.1	<0.10
CrMnNi	12.1	11.9	11.81	2.1	6.8	13.9	2.4	0.20
CrCoNi	8.7	8.2	8.06	44.4	6.8	10.7	1.4	0.20
FeMnMn	17.5	19.9	21.86	−32.3	19.5	5.7	<0.1	<0.10
FeMnCo	17.2	21.7	18.13	−75.6	9.4	3.4	0.3	6.30
FeFeFe	14.7	17.1	17.75	−52.2	12.2	1.3	<0.1	1.10
FeFeNi	12.6	15.2	14.75	−67.2	20.0	2.7	0.1	0.16

Definitions: Curie constant (C [emu K mol^{-1}]), Curie constant spin-only value (C_{SO} [emu K mol^{-1}]), Weiss constant (Θ), critical temperature (T_C), saturation magnetization (M_S), remnant magnetization at 2 K (M_R) and coercive field at 2 K (H_{Coer}). $S(Cr^{3+}) = 3/2$, $S(Fe^{3+}) = 5/2$, $S(Mn^{2+}) = 5/2$, $S(Fe^{2+}) = 3/2$, $S(Co^{2+}) = 3/2$, $S(Ni^{2+}) = 1$.

Accordingly, the resulting 2D magnetic network can be described as ferromagnetic Cr^{III}–Mn^{II} chains connected antiferromagnetically through Mn^{2+} bridges.

Additionally, when heated under controlled conditions, this family of molecule-based layered materials produce single-phase spinel-like mixed oxides ($M^{II}M_2{}^{III}O_4$), which exhibit ferrimagnetic ordering at higher temperatures than those of their molecular precursors. Among these products, the $(Mn,Co,Fe)_3O_4$ derivative, behaves as magnet above room temperature. This coordination chemistry approach towards the synthesis of oxides represents a substantial advance with respect to the standard ceramic method used so far.[94] The crystalline nature of the molecular precursors, which are subjected to thermal decomposition, leads to oxides with a high degree of homogeneity, which can be efficiently formed at relatively low temperatures (below 500 °C). Finally, the versatility of the oxalate chemistry could permit the production of a wide range of intermetallic oxides that at present are non-existent.

From a technological point of view, the solubility of these molecular precursors in water combined with their ability to produce magnetic spinel-like oxides, turns them into excellent vehicles for the nanostructuration of the latter onto surfaces through soft lithography techniques. As a proof of this concept, we succeeded in the sub-micrometric patterning of the room temperature magnetic $(Mn,Co,Fe)_3O_4$ spinel into ordered arrays of millimetre length stripes onto Si(100) substrates by means of lithographically controlled wetting (LCW).[92] Their magnetic response was confirmed with magnetic force microscopy (MFM) measurements (Fig. 30). This strategy opens the door for a wide range of unprecedented applications that were not accessible due to the poor solubility of the precursors employed so far in the synthesis of mixed oxides.

Reducing the dimensionality and controlling the magnetic behaviour of 1D crown ether-based bimetallic oxalate-bridged architectures: design of single chain magnets

So far we have shown that the general synthetic tools used in coordination chemistry to direct the assembly of molecular building-blocks can afford the preparation of bimetallic oxalate complexes with extended structures. Here we will show that the growth of these frameworks can be restricted to form bimetallic chains, for which a rich variety of magnetic behaviours are expected. To illustrate this approach we will recall the structure of the $[K(18\text{-crown-}6)]_3[M^{II}M^{III}(ox)_3]$ family as a starting point. A careful look at this structure allows us to predict that by removing the hydrogen bond interactions established between the M(II) and M(III) sites, one could obtain 1D oxalate-bridged bimetallic chains. Therefore, we focused on substituting these water molecules in the coordination sphere of the M(II) ions with bidentate organic capping ligands. With this idea in mind, we substituted the simple salt $MnCl_2$ with the complex $Mn(bpy)Cl_2$ (bpy = $C_{10}H_8N_2$) in the synthesis of $[K(18\text{-crown-}6)]_3[Mn_3(H_2O)_4\{Cr(ox)_3\}_3]$ and succeeded in the isolation of the chain compound $[K(18\text{-crown-}6)][Mn(bpy)Cr(ox)_3]$.[95]

This compound is made up of alternating anionic $[Mn(bpy)Cr(ox)_3]^-$ oxalate-bridged bimetallic chains and cationic $[K(18\text{-crown-}6)]^+$ complexes (Fig. 31). The anionic chain is composed of $[Cr(ox)_3]^{3-}$ complexes and Mn(II) ions bridged through the oxalate linker in its bis-bidentate chelating mode. Each Cr(III) centre is surrounded by two μ_2-bridging and one terminal oxalate ligands with regular octahedral coordination geometry. The Mn(II) metallic centres are octahedrally coordinated by two chelating oxalate ligands and an organic 2,2′-dipyridyl molecule. The metal centres along a given chain exhibit opposite chirality, with Cr(III) and Mn(II) centres adopting Λ and Δ configurations, following the pattern: ...ΛΔΛΔ... As expected, the substitution of the coordinating water molecules formerly bonded to the Mn(II) ions with the bipyridyl capping ligand gives rise to a better isolation between the chains. The removal of hydrogen bonding interactions means that the shortest interchain metal-to-metal distance in this compound increases to 7.8 Å, whilst the same parameter is rather smaller for the family $[K(18\text{-crown-}6)]_3[M^{II}M^{III}(ox)_3]$ (*ca.* 6.9 Å). As thoroughly outlined in this section, non-covalent interactions again play a determinant role in directing the packing of the cationic $[K(18\text{-crown-}6)]^+$ complexes. The electrostatic interaction between the metallic ion and the terminal oxalate ligand bonded to the Cr(III) centre (O···K = 2.687 Å) seems to be responsible for the eclipsed packing exhibited by the cationic units along the *a* axis. Regarding its magnetic properties, this bimetallic chain behaves as a quasi-1D Heisenberg ferromagnetic system, with no magnetic ordering above 2 K. This is mainly due to the increase in the distance separating the metal centres across the chain, which reduces the strength of the magnetic dipolar interactions operating between the chains.

Given that the magnetic isolation between the chains is one of the vital requirements for the observation of the atypical single chain magnet (SCM) behaviour,[96] this result pushed us to extend this same synthetic strategy to other metals and organic ligands in order to tune not only the distance separating these magnetic chains in the solid-state, but also other crucial parameters such as the nature and intensity of the magnetic exchange and/or the magnetic anisotropy across the chain. Our first step in this direction was the substitution of the isotropic Mn(II) with the highly anisotropic Co(II) ion. In contrast to our assumption, the resulting $[K(18\text{-crown-}6)][Co(bpy)Cr(ox)_3]$ polymorph[45] behaves as a soft ferromagnet below 6 K and does not exhibit slow relaxation of the

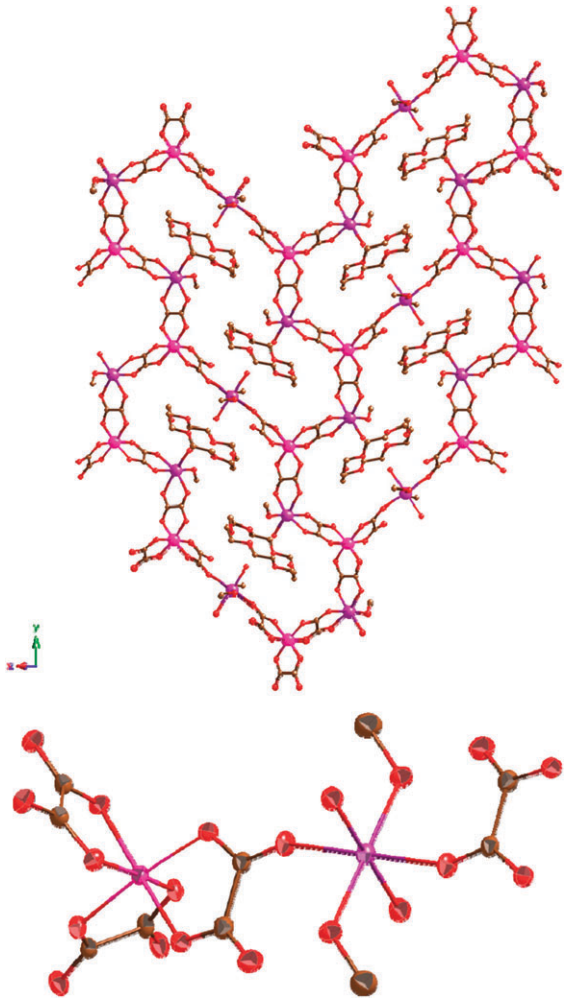

Fig. 29 Structure of the $\{[Mn(OH_2)(CH_3OH)][Mn(OH_2)_2]_2[Cr(ox)_3]_2$-(18-crown-6)$\}\cdot CH_3OH$ phase (*top*). Thermal ellipsoid representation (50% probability) of the unusual simultaneously bidentate and monodentate oxalate bridge (*bottom*). Cr (pink), Mn (purple), O (red) and C (black). Hydrogen atoms have been omitted for the sake of simplicity.

magnetization. Nevertheless, these preliminary result helped us to understand that, along with the distance separating the chains across the layers (d_{inter}), that separating these magnetic layers (d_{layer}) is equally important to control the magnetism in these 1D systems. In fact, d_{layer} = 7.2 Å is quite significantly smaller than d_{inter} = 10.7 Å in these compounds, suggesting that the magnetic dipolar interactions operating between layers are mainly responsible for the onset of bulk magnetic ordering in the Co(II) derivative. To prove this point, we aimed to isolate related chain compounds that, while maintaining d_{inter} almost unmodified, could exhibit larger d_{layer} values.

Minimum changes in the synthetic procedure, including the substitution of the 2,2′-bipyridyl with the 2,2′-dipyridylamine (Fig. 32), permitted us to isolate two isostructural compounds: $[K(18\text{-crown-6})][Co^{II}(dpy)M^{III}(ox)_3]$ (M^{III} = Cr, Fe; dpy = $C_{10}N_3H_9$; Fig. 31).[45] These systems behave as soft ferro- and ferrimagnets at 4.6 and 11 K, following the general trend observed in other bimetallic oxalate-based magnets, where the introduction of $[Cr(ox)_3]^{3-}$ units results in ferromagnetic interactions whilst the $[Fe(ox)_3]^{3-}$ complexes promote antiferromagnetic coupling. According to their AC dynamic magnetic measurements (Fig. 33), both systems exhibit a clear dependence of their in-phase and out-of-phase maxima with the frequency of the oscillating field. Nevertheless, the presence of SCM behaviour was ruled out on the basis of the Mydosh parameter (ϕ), which suggested glassy relaxation instead. Since the overall structure of these bimetallic chains are almost equivalent to those described above except for the d_{layer} parameter, which experiences a minor increment reaching 7.6 Å, we can consider it to be the main factor responsible for the changes observed in their magnetic properties.

This experimental evidence encouraged us to keep exploring the design of other related chain compounds which could exhibit even larger d_{layer} values. Our efforts bore fruit with the synthesis of the first oxalate-based SCM: $[K(18\text{-crown-6})]_{1/2}$-$[(18\text{-crown-6})(FC_6H_4NH_3)]_{1/2}[Co(H_2O)_2Cr(ox)_3]$ (Fig. 31).[97] In this case, the distance between the chains (d_{inter} = 7.6 Å) is even shorter than those exhibited by the previous examples, but the introduction of an additional cation to the multilayered structure, $[(18\text{-crown-6})(FC_6H_4NH_3)]^+$, causes the separation between the layers to increase up to 9.2 Å, and the intensity of the magnetic interactions operating between them are drastically reduced. Though in this system, the ferromagnetic Ising-like chains are supramolecularly

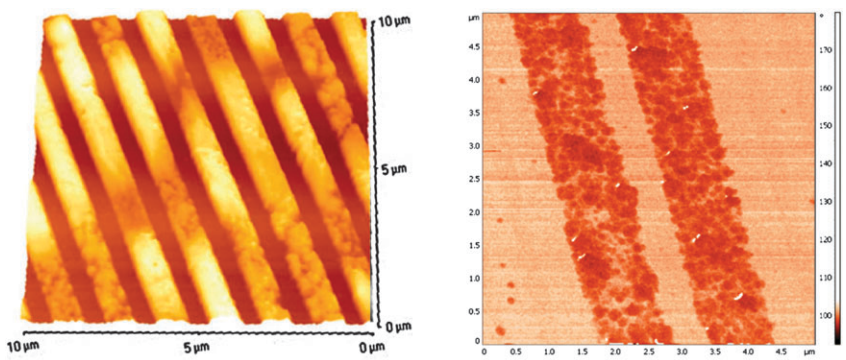

Fig. 30 AFM image (area of 10 × 10 μm^2) showing the patterning obtained from the deposition of a water solution of $[K(18\text{-crown-6})]_3$-$[Fe^{II}_{1.5}Co^{II}_{1.5}(H_2O)_4\{Fe^{III}(ox)_3\}_3]$ onto a Si(100) wafer by using the LCW technique (*left*). MFM phase image (area of 5 × 5 μm^2) showing the magnetic response of the printed lines at ambient conditions after thermal heating (*right*).

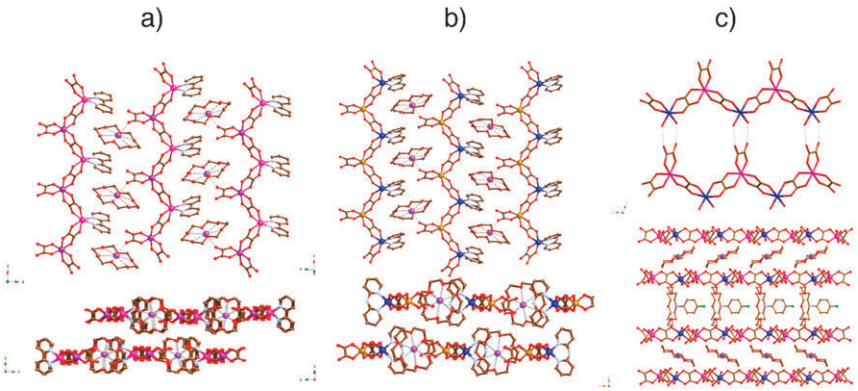

Fig. 31 View of the parallel arrangement of the bimetallic oxalate-bridged chains and perspective along the *a* axis showing the multilayered structure of (a) $[K(18\text{-crown-6})][M^{II}(bpy)Cr(ox)_3]$ (M^{II} = Mn, Co); (b) $[K(18\text{-crown-6})][Co^{II}(dpy)M^{III}(ox)_3]$ (M^{III} = Cr, Fe) and (c) $[K(18\text{-crown-6})]_{1/2}[(18\text{-crown-6})(FC_6H_4NH_3)]_{1/2}[Co(H_2O)_2Cr(ox)_3]$. Hydrogen atoms have been omitted for clarity.

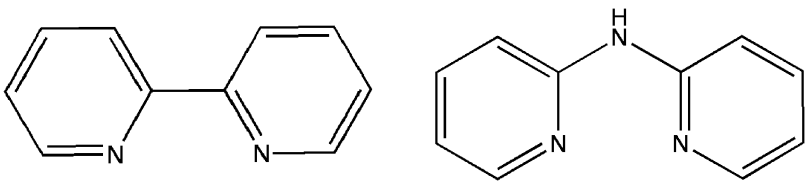

Fig. 32 Structure of the 2,2′-dipyridyl (bpy) and 2,2′-dipyridylamine (dpy) ligands.

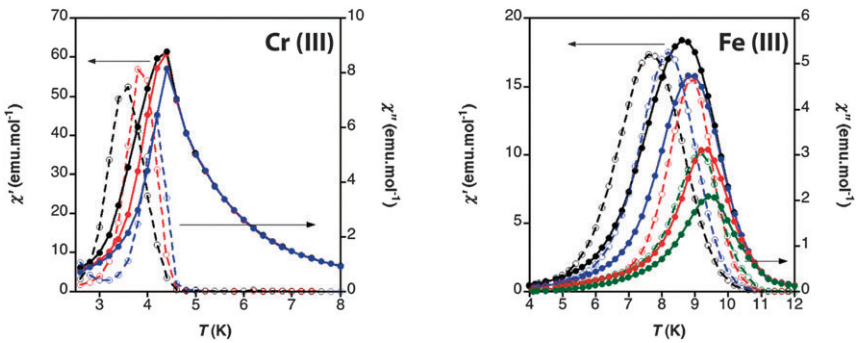

Fig. 33 AC susceptibility in the 1–1000 Hz interval for $[K(18\text{-crown-6})][Co^{II}(dpy)M^{III}(ox)_3]$ (M^{III} = Cr and Fe). In-phase susceptibility is represented by filled symbols whereas out-of-phase susceptibility is represented by empty ones. Solid lines are only a guide to the eye.

interlinked through hydrogen bonding interactions across the plane, the low efficiency of this sort of bridge in transmitting the magnetic exchange enables the observation of the slow relaxation of the isolated chains (Fig. 34). At this point, it is worthwhile remarking that the use of this ligand in the design of SCMs remained a challenging goal due to the smaller intrachain magnetic exchange mediated by the oxalate linker in comparison with other bridging linkers such as CN^- or N_3^-, which are more appropriate to fulfil the demanding requirements necessary to observe slow relaxation of the magnetization in low-dimensional systems.

Although the magnetic properties of these water-soluble CPs are obviously not retained in solution, the evaporation of the solvent can easily regenerate the starting products and consequently their magnetic properties. This unprecedented feature is in sharp contrast with the insolubility exhibited by the rest of the oxalate-based magnets reported so far. Furthermore, we can take advantage of this feature to prepare novel hybrid materials by means of intercalation chemistry. In this context, the use solid-state layered hosts of the family of layered double hydroxides (LDHs) has permitted the isolation of multilayered hybrids that combine their intrinsic magnetic properties with those provided by either low-dimensional oxalate-bridged polynuclear complexes or even 2D extended networks.[98,99] Finally, we have briefly described how this solubility can be used to process these magnets on surfaces through soft lithographic techniques in order to fabricate sub-micrometric patterns, which, by thermal treatment, can ultimately lead to nanostructures of mixed-oxide magnets.

5. Concluding remarks

The field of functional molecular materials has seen very rapid progress since the discovery of a variety of cooperative solid-state properties such as conductivity and superconductivity, non-linear optics, and ferromagnetism. Currently, one of the

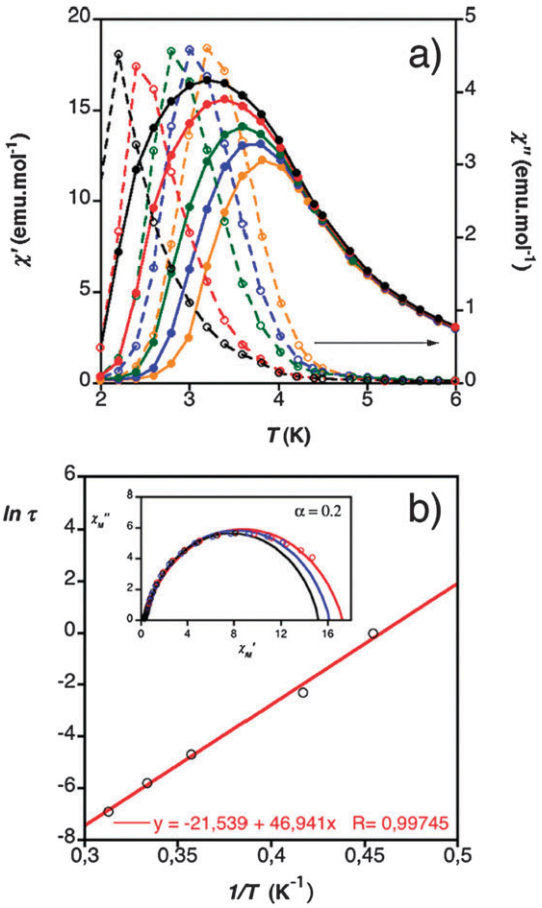

Fig. 34 Dynamic magnetic measurements of $[K(18\text{-crown-}6)]_{1/2}[(18\text{-crown-}6)(FC_6H_4NH_3)]_{1/2}[Co(H_2O)_2Cr(ox)_3]$. (a) AC susceptibility at 1 (black), 10 (red), 110 (blue), 332 (green) and 1000 Hz (orange). In-phase and out-of-phase signals are represented by filled and empty symbols, respectively. Solid lines are only a guide to the eye. (b) Best fitting (solid red line) of the out-of-phase maxima to the Arrhenius law giving: $\tau_0 = 4.4 \times 10^{-10}$ s^{-1} and $\Delta/K_B = 46.9$ K. The inset shows the Cole–Cole diagram collected at 2.4 (black), 2.3 (blue) and 2.2 K (red). Solid lines represent the best fit of the data to a Debye model. The obtained α values ranging in the 0.18–0.23 interval, are in excellent agreement with those expected for SCM-like relaxation.

most appealing aims is to create complex materials exhibiting multifunctional properties. In this aspect the possibilities offered by the molecular approach is unparalleled in the word of solid state chemistry. Thus, from a wise choice of molecular building blocks one can combine in the same crystal lattice two properties that are difficult or impossible to achieve in a conventional inorganic solid. A possible approach consists of building up two-network hybrid solids formed by two molecular fragments where each network furnishes distinct physical properties. If the two networks are quasi-independent, a coexistence of the two physical properties is anticipated. If, on the contrary, the two molecular networks are coupled, new properties should appear as a consequence of this interaction.

The examples reported here illustrate this concept. Thus, we have shown how the use of coordination chemistry and, in particular, the combination of magnetic oxalate-based coordination polymers with functional molecules, provides a suitable approach for designing hybrid magnetic materials exhibiting multifunctional properties.

In the first part hybrid magnets formed by an extended magnetic network of bimetallic oxalates and organic radicals have been reported. The role of these radicals is twofold: (a) they template the growth of the extended magnetic network leading to unprecedented structures for the bimetallic oxalato lattice (a 3D achiral network of helicoidal hexagonal channels, for example); (b) a weak but sizeable magnetic exchange interaction between these paramagnetic radicals and the ferromagnetic lattice has been detected by EPR, which influences the magnetism (coercive fields) in this family of magnets.

In the second part the bimetallic oxalates have been combined with spin crossover complexes in order to afford materials with coexistence of magnetic ordering and spin-crossover. This constitutes the first step towards the design of switching magnets in which the cooperative magnetism can be tuned by switching the spin state of the spin crossover molecule (*i.e.*, by applying an external stimulus).

In the third part we have taken advantage of the use of crown ethers to make soluble magnets of these coordination polymers. This possibility has allowed us to grow large crystals of these molecular magnets and to generate sub-micrometric patterning of these magnets on surfaces using soft lithography techniques. Additionally, we have shown that these patterns of low-T_C molecular magnets can be thermally decomposed to give rise to patterns of magnetic metal oxides which order above room temperature. Finally, we have shown that this family provides a nice example of crystal engineering in which the dimensionality of the magnetic lattice can be tuned at will. Thus, the dimensionality of these materials has been reduced from 2D to 1D, leading to the first example of a single-chain magnet based on the oxalate linker.

Acknowledgements

Financial support from the EU (SPINMOL ERC Advanced Grant to EC and IEF-253369 "MultiMOF" Marie Curie Fellowship to CMG), the Spanish Ministerio de Ciencia e Innovación (Project Consolider-Ingenio in Molecular Nanoscience and projects MAT2007-61584 and CTQ-2008-06720) and the Generalitat Valenciana (Prometeo Program) are gratefully acknowledged.

References

1 O. Kahn, *Molecular Magnetism*, VCH Publishers, Weinheim, 1993.
2 M. Pilkington and S. Decurtins, in *Magnetism: Molecules to Materials II: Models and Experiments*, ed. J. S. Miller and M. Drillon, Wiley, 2003, p. 339.
3 O. Kahn, Y. Pei, M. Verdaguer, J. P. Renard and J. Sletten, *J. Am. Chem. Soc.*, 1988, **110**, 782.
4 M. Shatruk, C. Avendano and K. R. Dunbar, *Prog. Inorg. Chem.*, 2009, **56**, 155.
5 M. Kurmoo and C. J. Kepert, *New J. Chem.*, 1998, **22**, 1515.
6 E. Coronado, J. R. Galán-Mascarós, C. J. Gómez-García and V. Laukhin, *Nature*, 2000, **408**, 447.
7 S. Bénard, P. Yu, J. P. Audiére, V. Riviére, R. Clèment, J. Ghilhelm, L. Tchertanov and K. Nakatani, *J. Am. Chem. Soc.*, 2000, **122**, 9444.
8 O. Sato, T. Iyoda, A. Fujishima and K. Hashimoto, *Science*, 1996, **272**, 704.

9 A. Bleuzen, C. Lomenech, V. Escax, F. Villain, F. Varret, C. Cartier and M. Verdaguer, *J. Am. Chem. Soc.*, 2000, **122**, 6648.
10 E. Coronado, M. C. Giménez-López, T. Korzeniak, G. Levchenko, F. M. Romero, A. Segura, V. García-Baonza, J. C. Cezar, F. M. F. de Groot, A. Milner and M. Paz-Pasternak, *J. Am. Chem. Soc.*, 2008, **130**, 15519.
11 M. Minguet, D. Luneau, E. Lhotel, V. Villar, C. Paulsen, D. B. Amabilino and J. Veciana, *Angew. Chem., Int. Ed.*, 2002, **41**, 586.
12 E. Coronado, C. J. Gómez-García, A. Nuez, F. M. Romero and J. C. Waerenborgh, *Chem. Mater.*, 2006, **18**, 2670.
13 N. Guillou, C. Livage, M. Drillon and G. Ferey, *Angew. Chem., Int. Ed.*, 2003, **42**, 5314.
14 C. Train, R. Gheorge, V. Krstic, L.-M. Chamoreau, N. S. Ovanesyan, G. L. J. A. Rikken, M. Gruselle and M. Verdaguer, *Nat. Mater.*, 2008, **7**, 729.
15 C. Train, T. Nuida, R. Gheorghe, M. Gruselle and S.-i. Ohkoshi, *J. Am. Chem. Soc.*, 2009, **131**, 16838.
16 E. Q. Gao, Y. F. Yue, S. Q. Bai, Z. He and C. H. Yan, *J. Am. Chem. Soc.*, 2004, **126**, 1419.
17 E. Coronado, C. J. Gómez-García, A. Nuez, F. M. Romero, E. Rusanov and H. Stoeckli-Evans, *Inorg. Chem.*, 2002, **41**, 4615.
18 K. Inoue, K. Kikuchi, M. Ohba and H. Okawa, *Angew. Chem., Int. Ed.*, 2003, **42**, 4810.
19 S. Ohkoshi, H. Tokoro, T. Matsuda, H. Takahashi, H. Irie and K. Hashimoto, *Angew. Chem., Int. Ed.*, 2007, **46**, 3238.
20 H. Cui, Z. Wang, K. Takahashi, Y. Okano, H. Kobayashi and A. Kobayashi, *J. Am. Chem. Soc.*, 2006, **128**, 15074.
21 G. Rogez, N. Viart and M. Drillon, *Angew. Chem., Int. Ed.*, 2010, **49**, 1921.
22 E. Coronado and P. Day, *Chem. Rev.*, 2004, **104**, 5419.
23 E. Coronado and J. R. Galán-Mascarós, *J. Mater. Chem.*, 2005, **15**, 66.
24 S. Kitagawa, R. Kitaura and S.-I. Noro, *Angew. Chem., Int. Ed.*, 2004, **43**, 2334.
25 C. J. Kepert, *Chem. Commun.*, 2006, 695.
26 O. Sato, *Acc. Chem. Res.*, 2003, **36**, 692.
27 D. Maspoch, D. Ruiz-Molina and J. Veciana, *J. Mater. Chem.*, 2004, **14**, 2713.
28 A. Alberola, E. Coronado, J. R. Galán-Mascarós, C. Giménez-Saiz and C. J. Gómez-García, *J. Am. Chem. Soc.*, 2003, **125**, 10774.
29 J. R. Galán-Mascarós, E. Coronado, P. A. Goddard, J. Singleton, A. I. Coldea, J. D. Wallis, S. J. Coles and A. Alberola, *J. Am. Chem. Soc.*, 2010, **132**, 9271.
30 H. Tamaki, Z. J. Zhong, N. Matsumoto, S. Kida, M. Koikawa, N. Achiwa, Y. Hashimoto and H. Okawa, *J. Am. Chem. Soc.*, 1992, **114**, 6974.
31 K. S. Min and J. S. Miller, *Dalton Trans.*, 2006, 2463.
32 E. Coronado, J. R. Galán-Mascarós and C. Martí-Gastaldo, *J. Mater. Chem.*, 2006, **16**, 2685.
33 R. Pellaux, H. W. Schmalle, R. Huber, P. Fischer, T. Hauss, B. Ouladdiaf and S. Decurtins, *Inorg. Chem.*, 1997, **36**, 2301.
34 C. Mathoniere, C. J. Nuttall, S. G. Carling and P. Day, *Inorg. Chem.*, 1996, **35**, 1201.
35 S. G. Carling, C. Mathoniere, P. Day, K. M. A. Malik, S. J. Coles and M. B. Hursthouse, *J. Chem. Soc., Dalton Trans.*, 1996, 1839.
36 C. Mathonière, S. G. Carling, Y. S. Dou and P. Day, *J. Chem. Soc., Chem. Commun.*, 1994, 1551.
37 H. Okawa, N. Matsumoto, H. Tamaki and M. Ohba, *Mol. Cryst. Liq. Cryst.*, 1993, **232**, 617.
38 S. Decurtins, H. W. Schmalle, P. Schneuwly and H. R. Oswald, *Inorg. Chem.*, 1993, **32**, 1888.
39 S. Decurtins, H. W. Schmalle, P. Schneuwly, J. Ensling and P. Gutlich, *J. Am. Chem. Soc.*, 1994, **116**, 9521.
40 M. Hernandez-Molina, F. Lloret, C. Ruiz-Perez and M. Julve, *Inorg. Chem.*, 1998, **37**, 4131.
41 E. Coronado, J. R. Galán-Mascarós, C. J. Gómez-García and J. M. Martínez-Agudo, *Inorg. Chem.*, 2001, **40**, 113.
42 F. Pointillart, C. Train, M. Gruselle, F. Villain, H. W. Schmalle, D. Talbot, P. Gredin, S. Decurtins and M. Verdaguer, *Chem. Mater.*, 2004, **16**, 832.
43 M. Clemente-León, E. Coronado, C. J. Gómez-García and A. Soriano-Portillo, *Inorg. Chem.*, 2006, **45**, 5653.
44 R. S. Fishman, M. Clemente-León and E. Coronado, *Inorg. Chem.*, 2009, **48**, 3039.
45 E. Coronado, J. R. Galán-Mascarós and C. Martí-Gastaldo, *CrystEngComm*, 2009, **11**, 2143.
46 S. Triki, F. Berezovsky, J. S. Pala, E. Coronado, C. J. Gómez-García, J. M. Clemente, A. Riou and P. Molinie, *Inorg. Chem.*, 2000, **39**, 3771.
47 F. D. Rochon, R. Melanson and M. Andruh, *Inorg. Chem.*, 1996, **35**, 6086.
48 N. Stanica, C. V. Stager, M. Cimpoesu and M. Andruh, *Polyhedron*, 1998, **17**, 1787.
49 G. Marinescu, M. Andruh, R. Lescouëzec, M. C. Muñoz, J. Cano, F. Lloret and M. Julve, *New J. Chem.*, 2000, **24**, 527.
50 E. Coronado, M. C. Giménez, C. J. Gómez-García and F. M. Romero, *Polyhedron*, 2003, **22**, 3115.
51 E. Coronado, J. R. Galán-Mascarós and C. J. Gómez-García, *J. Chem. Soc., Dalton Trans.*, 2000, 205.
52 S. Rashid, S. S. Turner, P. Day, M. E. Light and M. B. Hursthouse, *Inorg. Chem.*, 2000, **39**, 2426.
53 E. Coronado, J. R. Galán-Mascarós, C. Giménez-Saiz, C. J. Gómez-García, C. Ruiz-Pérez and S. Triki, *Adv. Mater.*, 1996, **8**, 737.
54 M. Clemente-León, E. Coronado, J. R. Galán-Mascarós and C. J. Gómez-García, *Chem. Commun.*, 1997, 1727.
55 E. Coronado, J. R. Galán-Mascarós, C. J. Gómez-García, J. Ensling and P. Gütlich, *Chem.–Eur. J.*, 2000, **6**, 552.
56 G. Ballester, E. Coronado, C. Giménez-Saiz and F. M. Romero, *Angew. Chem., Int. Ed.*, 2001, **40**, 792.
57 A. Alberola, E. Coronado, C. Giménez-Saiz, C. J. Gómez-García, F. M. Romero and A. Tarazón, *Eur. J. Inorg. Chem.*, 2005, 389.
58 K. Awaga, T. Inabe, U. Nagashima, T. Nakamura, M. Matsumoto, Y. Kawabata and Y. Maruyama, *Chem. Lett.*, 1991, 1777.
59 A. Yamaguchi, K. Awaga, T. Inabe, T. Nakamura, M. Matsumoto and Y. Maruyama, *Chem. Lett.*, 1993, 1443.
60 C. Michaut, L. Ouahab, P. Bergerat, O. Kahn and A. Bousseksou, *J. Am. Chem. Soc.*, 1996, **118**, 3610.
61 H. Imai, T. Otsuka, T. Naito, K. Awaga and T. Inabe, *J. Am. Chem. Soc.*, 1999, **121**, 8098.
62 H. O. Stumpf, L. Ouahab, Y. Pei, D. Grandjean and O. Kahn, *Science*, 1993, **261**, 447.
63 M. G. F. Vaz, L. M. M. Pinheiro, H. O. Stumpf, A. F. C. Alcântara, S. Golhen, L. Ouahab, O. Cador, C. Mathonière and O. Kahn, *Chem.–Eur. J.*, 1999, **5**, 1486.
64 U. Geiser, B. L. Ramakrishna, R. D. Willett, F. B. Hulsbergen and J. Reedijk, *Inorg. Chem.*, 1987, **26**, 3750.
65 H. Oshio and U. Nagashima, *Inorg. Chem.*, 1992, **31**, 3295.
66 M. Drillon, E. Coronado, D. Beltrán and R. Georges, *Chem. Phys.*, 1983, **79**, 449.
67 A. Tarazón, C. Giménez-Saiz, C. J. Gómez-García and F. M. Romero, *Molecules*, 2004, **9**, 782.
68 P. Gütlich, A. Hauser and H. Spiering, *Angew. Chem., Int. Ed. Engl.*, 1994, **33**, 2024.
69 J. A. Real, A. B. Gaspar and M. C. Muñoz, *Dalton Trans.*, 2005, 2062.
70 R. Sieber, S. Decurtins, H. Stoeckli-Evans, C. Wilson, D. Yufit, J. A. K. Howard, S. C. Capelli and A. Hauser, *Chem.–Eur. J.*, 2000, **6**, 361.
71 H. Z. Kou and O. Sato, *Inorg. Chem.*, 2007, **46**, 9513.
72 E. Coronado, J. R. Galán-Mascarós, M. C. Giménez-López, M. Almeida and J. C. Waerenborgh, *Polyhedron*, 2007, **26**, 1838.
73 M. Clemente-León, E. Coronado, M. C. Giménez-López, A. Soriano-Portillo, J. C. Waerenborgh, F. S. Delgado and C. Ruiz-Pérez, *Inorg. Chem.*, 2008, **47**, 9111.
74 M. Clemente-León, E. Coronado, M. López-Jordà, G. Mínguez Espallargas, A. Soriano-Portillo and J. C. Waerenborgh, *Chem.–Eur. J.*, 2010, **16**, 2207.
75 R. Pritchard, S. A. Barrett, C. A. Kilner and M. A. Halcrow, *Dalton Trans.*, 2008, 3159.
76 M. Clemente-León, E. Coronado and M. López-Jordà, *Dalton Trans.*, 2010, **39**, 4903.
77 M. Gruselle, C. Train, K. Boubekeur, P. Gredin and N. Ovanesyan, *Coord. Chem. Rev.*, 2006, **250**, 2491 and references therein.

78 H. Okawa, A. Shigematsu, M. Sadakiyo, T. Miyagawa, K. Yoneda, M. Ohba and H. Kitagawa, *J. Am. Chem. Soc.*, 2009, **131**, 13516.
79 M. Clemente-León, E. Coronado and M. López-Jordà, unpublished results.
80 M. Clemente-León, E. Coronado, M. López-Jordà, C. Desplanches, S. Asthana, H. Wang and J.-F. Létard, manuscript in preparation.
81 S. Hayami, Z.-Z. Gu, M. Shiro, Y. Einaga, A. Fujishima and O. Sato, *J. Am. Chem. Soc.*, 2000, **122**, 7126.
82 G. Juhász, S. Hayami, O. Sato and Y. Maeda, *Chem. Phys. Lett.*, 2002, **364**, 164.
83 S. Hayami, K. Hiki, T. Kawahara, Y. Maeda, D. Urakami, K. Inoue, M. Ohama, S. Kawata and O. Sato, *Chem.–Eur. J.*, 2009, **15**, 3497.
84 C. Enachescu, A. Hauser, J.-J. Girerd and M.-L. Boillot, *ChemPhysChem*, 2006, **7**, 1127.
85 E. Coronado, J. R. Galán-Mascarós, C. J. Gómez-García and C. Martí-Gastaldo, *Inorg. Chem.*, 2005, **44**, 6197.
86 F. M. Romero, R. Ziessel, M. Bonnet, Y. Pontillon, E. Ressouche, J. Schweizer, B. Delley, A. Grand and C. J. Paulsen, *J. Am. Chem. Soc.*, 2000, **122**, 1298.
87 E. Coronado, J. R. Galán-Mascarós and C. Martí-Gastaldo, *Inorg. Chem.*, 2006, **45**, 1882.
88 E. Coronado, J. R. Galán-Mascarós, C. Martí-Gastaldo, J. C. Waerenborgh and P. Gaczynski, *Inorg. Chem.*, 2008, **47**, 6829.
89 E. Coronado and C. Martí-Gastaldo, unpublished results.
90 J. Cirujeda, L. E. Ochando, J. M. Amigo, C. Rovira, J. Rius and J. Veciana, *Angew. Chem., Int. Ed. Engl.*, 1995, **34**, 55.
91 E. Coronado, J. R. Galán-Mascaros and C. Martí-Gastaldo, *Inorg. Chem.*, 2007, **46**, 8108.
92 E. Coronado, C. Martí-Gastaldo, J. R. Galán-Mascaros and M. Cavallini, *J. Am. Chem. Soc.*, 2010, **132**, 5456.
93 E. Coronado, J. R. Galán-Mascaros and C. Martí-Gastaldo, *Inorg. Chim. Acta*, 2008, **361**, 4017.
94 E. Coronado, J. R. Galán-Mascaros and C. Martí-Gastaldo, Polímeros de coordinación solubles homo y heterometálicos basados en el ligando oxalato y método de obtención de espinelas a partir de ellos. *Patent WO2009130359-A1*, 2000.
95 E. Coronado, J. R. Galán-Mascarós and C. Martí-Gastaldo, *Polyhedron*, 2007, **26**, 2101.
96 C. Coulon, H. Miyasaka and R. Clérac, *Struct. Bonding*, 2006, **122**, 163 and references therein.
97 E. Coronado, J. R. Galán-Mascarós and C. Martí-Gastaldo, *J. Am. Chem. Soc.*, 2008, **130**, 14987.
98 E. Coronado, J. R. Galán-Mascarós, C. Martí-Gastaldo and A. Ribera, *Chem. Mater.*, 2006, **18**, 6112.
99 E. Coronado, C. Martí-Gastaldo, E. Navarro-Moratalla, A. Ribera and J. R. Galán-Mascarós, *J. Mater. Chem.*, 2010, **20**, 9476.